FOLDING AND COLORING PROBLEMS
IN MATHEMATICS AND PHYSICS

P. DI FRANCESCO

ABSTRACT. We review various folding problems arising in the physics of membranes and polymers. These are (1) the phantom folding of tethered membranes, i.e. the two-dimensional lattice folding; (2) the phantom folding of fluid membranes, i.e. the folding of tessellations of arbitrary genus; (3) the self-avoiding folding of polymers, i.e. the meander problem. All three problems are found to be related to coloring problems and possess one kind of underlying integrable structure, in different guises. Many mathematical results follow from taking advantage of this fact.

1. Introduction

In this work, we will deal with mathematical models describing mainly the so-called polymerized membranes and polymers. Examples of polymerized membranes in nature are for instance the hulls of the corpuscles of blood; polymers may be viewed among other things as the simplified physical counterparts of biological proteins. We believe in general that the study of polymerized objects will help our understanding of biological systems and processes, e.g. by predicting their favored geometrical shapes or configurations.

A membrane has a microscopic structure very close at least locally to that of a two-dimensional lattice, vertices being materialized by atoms and edges by chemical bonds. The simplest model for a membrane we can think of is precisely say the triangular lattice in $\mathbb{R}^2$ (see Fig. 1 (a)). Note that we may introduce irregularities in the structure of the membrane, such as curvature defects for instance. In all generality, the membranes are usually defined to belong to either of the two following classes:

  (i) **Tethered membranes:** these are regular networks, modelled by two-dimensional lattices (c.f. Fig. 1 (a));
 (ii) **Fluid membranes:** these are irregular networks, with arbitrary vertex valencies, and include the possibility for the membrane to form the tessellation of a surface of arbitrary topology (c.f. Fig. 1 (b), where the membrane has an underlying surface of genus 1, a torus).

When constructing models for membranes, we may include all sorts of physical ingredients that make them more realistic. For instance, introducing the possibility for the bonds to have short variations in length and attaching an elastic energy to these variations (bonds are modelled by small springs with a given rigidity constant), it has been possible to predict a geometrical "crumpling" transition [1] between two very different states of the membranes, either mainly flat or mainly compactly folded onto itself. Other models "forget" about the microscopic structure of the membranes and describe them rather as random surfaces embedded in $\mathbb{R}^3$, in a field-theoretic manner. Remarkably, the above-mentioned crumpling transition was also predicted in this continuous description, both analytically [2], [3], [4] and numerically [5].

(a)   (b)

(c)

FIGURE 1. Typical examples of polymerized objects: (a) tethered membrane, (b) fluid membrane wrapped on a torus, (c) polymer.

In the present study, we will not go into these technical sophistications, but rather concentrate on discrete (as opposed to continuous) models for tethered or fluid membranes with rigid bonds between their atoms, hence which can be viewed as regular or irregular networks of vertices linked by edges of fixed length. The only possibility for such a membrane to modify its spatial configuration is through *folding* along its bonds, serving as hinges between adjacent faces. Even without any notion of energy cost for a membrane to change its spatial configuration, there are a number of interesting questions one can ask, related to how many folded configurations are accessible, or whether the membrane is foldable at all. We are going to deal mainly with such questions [6], [7], [8]. To go beyond this would require including more ingredients than just the geometry of the membrane. Typically one can attach to each configuration of the membrane a certain energy, function say of the rigidity of the membrane (it costs some energy to fold a bond), and then further study the behavior of the membrane when the temperature varies [9], [10], [11].

The aim of these notes is to present a general mathematical and physical framework for the study of various membrane folding problems, or their one-dimensional version, the polymer (or protein) folding problem. In the latter, the membrane is replaced by a chain made of n identical constituents which may be viewed as line segments of fixed length, in which the joints between two adjacent segments serve as hinges (see Fig.1 (c)). A fundamental question when dealing with folding problems is that of *self-avoidance*, namely: (i) is the object we fold transparent to itself (and therefore can interpenetrate itself; we then speak of *phantom folding*), or (ii) does it have steric constraints that prevent the object from interpenetrating itself (we then speak of *self-avoiding folding*). We will see that the effects of self-avoidance on discrete folding models can be extremely complex: already in one dimension, the question amounts to solving the "meander" problem and its cousins, one of the few open puzzles of the past century. Indeed, this is an old problem: it can probably be traced back to some work by Poincaré (1911), and reemerged in various contexts since: as mathematical recreation [24], as folding problem [25], [26], in relation to the 16th Hilbert problem [27], in the theory of invariants of 3-manifolds [28], in abstract algebraic terms [31], [32], and in its own right [29], [30].

We will therefore only consider the phantom folding of membranes, the object of study of Sect.2 (tethered membrane folding) and Sect.3 (fluid membrane folding). In one dimension, however, phantom folding turns out to be trivial; we will therefore study the self-avoiding folding of polymers in Sect.4 below. Let us briefly describe the topics discussed in this paper.

Sect.2 : Tethered Membrane Folding. This first problem boils down to the study of folding of two-dimensional lattices of vertices linked by edges of given length, into $\mathbb{R}^d$, as particular maps from the lattice to $\mathbb{R}^d$. To make the models tractable, we will impose a discreteness condition that only finitely many local foldings are allowed. This in turn amounts to imposing that the target space be a d-dimensional lattice in $\mathbb{R}^d$, compatible with the lattice we are folding. After classifying the foldable lattices and their targets, we will address the problem of counting the number of folding configurations of a finite portion of the lattice (the membrane). It turns out that all these problems can be reformulated as coloring problems on some related two-dimensional lattice (in which edges must be painted using a given number of colors, with some specific constraints and weights to be

attached to coloring configurations). This relation between folding and coloring seems to be quite universal in the subject. We will concentrate on two particular lattice folding problems, namely when the lattice is the triangular lattice and the square-diagonal lattice (square lattice with the two diagonals of each square face drawn). The first problem turns out to be integrable, in the sense that it can be mapped onto an *integrable lattice model*, solved by *Bethe Ansatz* techniques, namely by diagonalizing explicitly a large (so-called transfer) matrix, encoding all the combinatorial data of the model. The notion of integrability here means that the model can be decorated by some parameters in such a way that, although the above transfer matrix changes, its eigenvectors don't; the model has therefore an underlying infinite family of commuting transfer matrices. In the other case, we will unearth the underlying algebraic structure of the folding model, rephrased as a so-called *fully-packed loop model* on the square lattice, and express it in terms of two copies of the Temperley-Lieb algebra, an essential tool of both integrable lattice models and link invariants. This algebra is indeed used to define the transfer matrices of the so-called six-vertex and Potts models on the square lattice, both integrable. This structural link to integrability is the main and most striking feature of this study.

Sect.3 : Fluid Membrane Folding. This second problem boils down to the study of folding of random tessellations of surfaces of arbitrary topology, by use of irregular networks of vertices linked by rigid bonds. We will concentrate on random triangulations and work out a generating function for the foldable triangulations, allowing us to enumerate them for fixed topology and area. This generating function is constructed by use of an integral over Hermitian matrices of given size N, computed by diagrammatic techniques borrowed from the theory of the functional integral. Using this integral representation, we will prove that the generating function is a solution of some discrete Hirota Bilinear equation, a central object in the modern study of integrable lattice models. In the large N limit corresponding to genus zero triangulations, this becomes a Hirota Bilinear partial differential equation of the same type as those found in KdV and KP hierarchies of integrable systems of partial differential equations. There, integrability means the existence of an infinite family of commuting flows, describing the evolution in infinitely many time variables of a function. So again integrability will show indirectly, and in a different albeit related manner.

   The actual folding problem of random triangulations lies one step further and will only be formulated as a matrix integral, but not solved by lack of good techniques.

Sect.4 : Polymer Folding. This third problem deals with the counting of compact self-avoiding folding configurations of a closed or open polymer. By compact we mean that the polymer must be folded onto just one of its edges, but self-avoidance means that we will distinguish the various ways in which this is realized. So, although a one-dimensional problem, the self-avoidance makes it two-dimensional in the sense that we must follow the path from the initial object to its compactly folded configuration in a plane. We will start by relating this problem to that of enumerating *meanders*, i.e. planar configurations of non-intersecting and non-self-intersecting loops (roads) crossing a line (river) through a given number of simple intersections (bridges), up to topological equivalence.

   We will present a few of the known formulations of the meander problem: first in purely combinatorial terms within the framework of the symmetric group, then

as a Hermitian multi-matrix integral of the same type as that used for counting foldable fluid triangulations, and finally as the gravitational version of a fully-packed loop model of the same type as that used in the folding problem of the square-diagonal lattice. By gravitational, we mean the replacement of the lattice by a statistical sum over all possible fluctuations of this lattice into tessellations of surfaces of arbitrary genera. The latter approach proves extremely powerful, though not completely rigorous, and allows us to predict exact values for the meander and related configuration exponents in the limit of a large number of bridges.

We will then reformulate the meander counting problem within the framework of the Temperley-Lieb algebra (the same as above!), and derive various bounds and estimates, as well as the value of the meander determinant, a meander-related quantity of interest.

The reemergence of an underlying structure common to many integrable models is the most remarkable outcome of this study. We are tempted to identify the level of complexity (and certainly the algebraic structure) of the two-dimensional phantom folding problems and the one-dimensional self-avoiding problems. In more physical terms, we will see that the meander problem, i.e. the polymer self-avoiding folding problem, is nothing but the gravitational version of a lattice model very close in its definition to the class of lattice phantom folding problems. The correct relation would be therefore something like: 1D self-avoiding folding $\equiv$ 2D phantom folding + gravity. The integrable structure is then simply observed to survive the coupling to gravity.

2. Tethered membrane folding: Lattices

2.1. Two-Dimensional Phantom Folding. Tethered membranes are regular two-dimensional networks of vertices connected by bonds. If we assume that the bonds are rigid, the only way for such an object to change its spatial configuration is through folding. The abstract definition of folding must match the intuitive idea that the bonds serve as hinges between their adjacent faces, which remain rigid. By membrane folding problem, we mean the study of its *folded configurations*, namely the final form of the folded network. This means that we are not taking into consideration the different *ways* of getting to that final state, nor do we require that the folding state be actually reachable without the membrane interpenetrating itself. This is usually called *phantom folding*, as the membrane is transparent to itself in the folding process. The study of folding of *self-avoiding* membranes is considerably more difficult, as it requires us to construct the path in three-dimensional space which connects the flat membrane to its folded configuration. This will however be addressed in detail in Sect.4 below in the case of one-dimensional objects, the polymers.

We are now ready for a mathematical definition of folding. We consider a finite subset S of a two-dimensional lattice of vertices linked by edges (rather viewed as a graph). A two-dimensional folding configuration of the lattice is a continuous map $\rho : S \rightarrow \mathbb{R}^2$ which preserves all the lengths of the edges of S. To avoid over-counting, ρ is considered up to any translation, rotation and reflection of the plane.

With this definition, the flat state of the membrane corresponds to $\rho = Id$. Next we must make sure the model is non-trivial, namely that non-trivial ρ's exist. This leads to the notion of *foldability*. It is clear for instance that any finite subset of
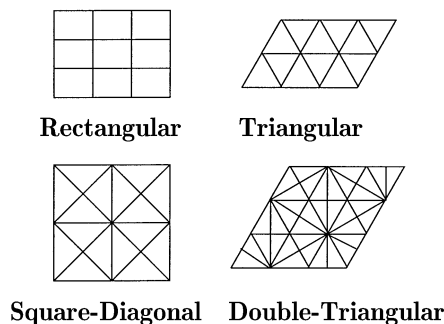
FIGURE 2. The classification of two-dimensional compactly fold-
able lattices.

the square lattice is foldable, as we might take for ρ any composition of reflections
wrt lattice lines. To have some physical relevance, a folding problem should have
many distinct folding configurations: this is usually required for allowing interesting
(geometrical) phase transitions. We will actually require that the membrane may
be *completely* folded onto one of its faces. This restricts very strongly the possible
form of the membrane to be folded: indeed, the corresponding two-dimensional
lattice has only one type of face, together with its finitely many possible rotations
and reflections. We will call this the requirement of *compact foldability*.

   This gives rise to the following classification theorem.

Theorem 1. *The two-dimensional compactly foldable lattices fall into the four
cases depicted in Fig. 2, namely: rectangular, triangular, square-diagonal and
double-triangular.*

   The proof goes as follows. Let us concentrate on a vertex of the lattice. Each
adjacent edge may serve as a hinge in the folding of its two adjacent faces, hence
bissects its two neighboring edges. Moreover, if an edge is folded, it must cross the
vertex; hence the edges are symmetric wrt the vertex. Each vertex v is therefore
the center of a regular star of say $2m_v$ edges forming angles of π/m_v, $m_v \geq 2$; hence
those angles are either right or acute. The faces are therefore polygons with at most
4 edges, and they can have 4 only if they are rectangles. This is the case where
all $m_v = 2$, the rectangular lattice. Otherwise, all faces must be triangular, with
right or acute angles. Such a face has angles $\pi/m_1, \pi/m_2, \pi/m_3$, with $m_i \geq 2$, and
$\sum 1/m_i = 1$. There are only three solutions up to permutation for (m_1, m_2, m_3),
namely

$$(3,3,3) \rightarrow \text{ Triangular}$$
(2.1)
$$(2,4,4) \rightarrow \text{Square-Diagonal}$$
$$(2,3,6) \rightarrow \text{Double-Triangular}$$

2.2. Entropy of Folding. In the following, we will restrict ourselves to the cases
of Fig.2. The first step in studying membrane folding is to try to enumerate the
folding configurations of each model. Let $N = PQ$ denote the number of faces
of a rectangular membrane made of P rows of Q faces: in the limit of large P, Q
(the thermodynamic limit) the number of folding configurations $Z_{P,Q}$ (also called
partition function) is expected on physical grounds to behave as z^N for some real

number $z \geq 1$, referred to as thermodynamic partition function per face. One also defines the thermodynamic entropy of folding per face

$$(2.2) \qquad s \; = \; \lim_{P,Q \to \infty} \frac{1}{PQ} \operatorname{Log} Z_{P,Q}.$$

Note that this number does not depend on the precise form of S, provided it contains arbitrarily large rectangles $P \times Q$. It is characteristic of the number of ways of folding S for bulky enough S, and depends only on the lattice of which S is a subset. We have $s = \operatorname{Log} z$.

In the case of the rectangular lattice, we simply have $s = 0$. Indeed, consider a rectangle of $P \times Q$ faces. A folding configuration is entirely specified by the list of all folded bonds. But once a bond is folded, the whole line to which it belongs must be too. Each horizontal line may be folded or not, as well as each vertical line: this results in a partition function $Z_{P,Q} = 2^{P+Q-2}$, and we get $s = 0$. So from a physical point of view, the rectangular folding problem is not interesting, as it has too few folding configurations. In the next sections, we study the other models, which all turn out to have $s > 0$.

2.3. Formulations as Vertex or Face Models.

The folding configurations of a given lattice are entirely determined by the list of its folded bonds. But these cannot be arbitrarily folded; they must satisfy a set of local constraints. For instance, the bonds adjacent to a four-valent vertex may only be in one of the 4 following folding configurations (i.e. much less than the $2^4 = 16$ possibilities a priori)

$$(2.3)$$
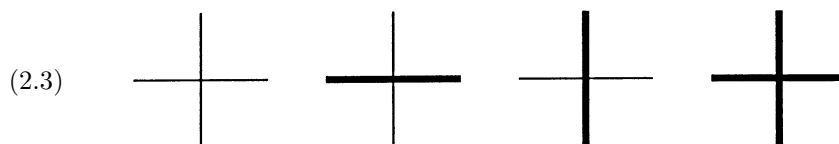
where we have represented in thick line the folded bonds. Around a 6-valent vertex the bonds may be in any of the following 11 folding configurations (to be compared with the $2^6 = 64$ possibilities a priori)

$$(2.4)$$

(1)   **(3)**   **(6)**   **(1)**
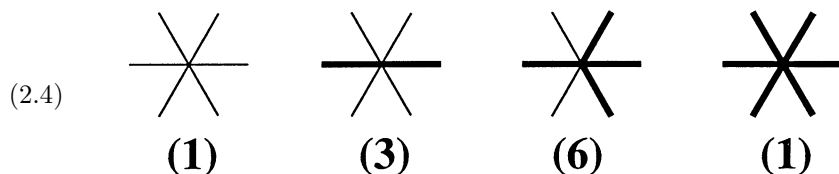
where we have indicated the number of distinct rotated configurations. More generally, around a $2m$-valent vertex, the bonds may be in only

$$(2.5) \qquad V_{2m} \; = \; 1 + \binom{2m-1}{m}$$

distinct folding configurations. To see why, assign unit vectors $\vec{u}_0, \vec{u}_1, ..., \vec{u}_{2m-1}$ parallel to each edge adjacent to the vertex, and pointing out of the vertex. It is useful to write them as $\vec{u}_i$, $i \in \mathbb{Z}_{2m}$, to emphasize that $\vec{u}_0 = \vec{u}_{2m}$ and $\vec{u}_{2m-1}$ are neighbors. A folding configuration of the vertex is a mapping $\rho : \{\vec{u}_i\} \to \{\vec{u}_i\}$, preserving the faces, namely such that the images of two neighboring edge vectors $(\vec{u}_i, \vec{u}_{i+1})$ are two neighboring edge vectors, say $(\vec{u}_j, \vec{u}_{j\pm1})$. Enumerating these maps amounts to enumerating the number of sequences of the $2m$ images around

the vertex, subject to this constraint. Introducing the cyclic graph $\mathcal{A}_{2m}$ with $2m$ vertices indexed by $i \in \mathbb{Z}_{2m}$, with adjacency matrix

$$(2.6) \qquad\qquad A_{i,j} = \delta_{j,i+1} + \delta_{j,i-1} \quad i,j \in \mathbb{Z}_{2m}$$

with the value 1 if i and j are connected by an edge, 0 otherwise, our problem boils down to the counting of the closed paths of length $2m$ on $\mathcal{A}_{2m}$. This number is simply

$$(2.7) \qquad\qquad N_{2m} = \mathrm{Tr}(A^{2m}).$$

To find V_{2m} we must divide this by the number $4m$ of choices for the origin and first step of the path, which amounts to fixing the face adjacent to $\vec{u}_0$ and $\vec{u}_1$. Fixing the origin and the first step, there is only one path wrapping around the cycle. All others are arbitrary successions of clockwise and counterclockwise steps, in equal numbers. As the first step is fixed say to be counterclockwise, this leaves us with the choice of the m clockwise steps among the $2m - 1$ remaining ones, hence $\binom{2m-1}{m}$ paths, and (2.5) follows. In view of the classification of Fig.2, we only need to know the $V_4 = 4$, $V_6 = 11$, $V_8 = 36$ and $V_{12} = 463$ vertex configurations. The corresponding folding problem is a vertex model; namely each folding configuration is obtained by assigning to each vertex of S one of the allowed vertex configurations in a globally compatible way, i.e. such that each edge (adjacent to two such vertices) has a well defined state, folded or unfolded. Note that in the two last cases of Fig.2, the vertex model is inhomogeneous, as we have two or three distinct types of vertices. This formulation proves however to be very tedious for both analytical and numerical studies.

In the following, we will approach all the models in a different way, by first defining *tangent vectors* $\vec{t}$ to the membrane, namely vectors which are parallel to its edges and with the same length, and oriented in such a way that the sum of tangent vectors around each face vanishes. For each membrane, there are two choices of these vectors (up to reversal of all directions). The local face condition

$$(2.8) \qquad\qquad \sum_{\text{face}} \vec{t} = \vec{0}$$

expresses the rigidity of the faces. By our definition of folding, this constraint must be preserved under any folding map ρ; namely we must have

$$(2.9) \qquad\qquad \sum_{\text{face}} \rho(\vec{t}) = \vec{0}$$

around each face of the membrane. This condition is actually a necessary and sufficient condition for $\rho : S \to \mathbb{R}^2$ to lead to a two-dimensional phantom folding configuration of the membrane. In all cases of Fig.2, there are only finitely many possible images $\rho(\vec{t})$ of tangent vectors, allowing for a reformulation of the problem as a face model, with finitely many possible configurations of the tangent vectors around a face. This is much better for both analytical and numerical study.

2.4. Folding of the Triangular Lattice. Let us consider the triangular lattice, with edges of unit length. With the choice of tangent vectors indicated in Fig.3 (a), a folding of the triangular lattice is a continuous map $\rho : S \to \mathbb{R}^2$, preserving the length of the tangent vectors and satisfying the condition (2.9) around each triangular face of S. Let $\vec{t}_1, \vec{t}_2, \vec{t}_3$ denote the unit tangent vectors to a given face of S. Their images $\rho(\vec{t}_i)$ are three unit vectors with vanishing sum, according to
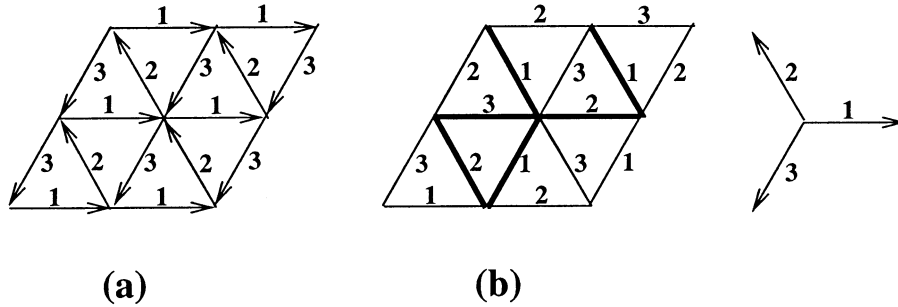
(a)   **(b)**

FIGURE 3. A choice (a) for the tangent vectors of the triangular lattice, together with the corresponding coloring of the edges by $1, 2, 3$. This is the flat configuration of the membrane. A folding configuration (b) with the corresponding folded bonds (thick black lines) and edge coloring. The three colors correspond to the three unit vectors with vanishing sum represented above.

the face rule (2.9). Fixing the image of one tangent vector of S to be a given unit vector $\vec{e_1}$, we see that the images of the tangent vectors of S may take only three values, $\vec{e_1}, \vec{e_2}, \vec{e_3}$, where $\vec{e_1}, \vec{e_2}, \vec{e_3}$ are three unit vectors with vanishing sum, hence forming angles of $2\pi/3$. Let us associate colors numbered $1, 2, 3$ to these three possible images.

A folding map ρ of the triangular lattice is therefore a coloring of its edges, with the three colors $1, 2, 3$, such that the three colors of edges around each face are all distinct. An example of such a coloring is given in Fig.3 (b) together with the corresponding folding configuration. The dual of this coloring model is the problem of tri-coloring the edges of the hexagonal (honeycomb) lattice in such a way that the three edges adjacent to each vertex are painted with distinct colors $1, 2, 3$. It has been solved by Baxter [12], by use of the Bethe Ansatz. Baxter's results yield in particular the exact value for the thermodynamic entropy of folding per face of the triangular lattice:

Theorem 2.

$$(2.10) \qquad\qquad s_T = Log\left(\frac{\sqrt{3}}{2\pi}\Gamma(1/3)^{3/2}\right).$$

This was originally proved by explicitly diagonalizing a large (transfer) matrix, indexed by the coloring configurations of rows of Q edges in the honeycomb lattice, and describing the "row-to-row transfer", i.e. the allowed coloring configurations for two such neighboring rows. The thermodynamic entropy (2.10) is then the logarithm of the largest (Perron-Frobenius) eigenvalue of this matrix. The diagonalization is performed using a particular ansatz for the form of the eigenvectors, the Bethe Ansatz. The proof of (2.10) being highly technical, we will not reproduce it here, but refer the interested reader to the original paper [12]. Let us simply mention that this model is part of the class of Two-dimensional Integrable Lattice Models, for which a Bethe Ansatz solution exists.

2.5. Folding of the Square-Diagonal Lattice. The Square-Diagonal lattice is made of triangular faces with one "long" edge of unit length and two "short" edges
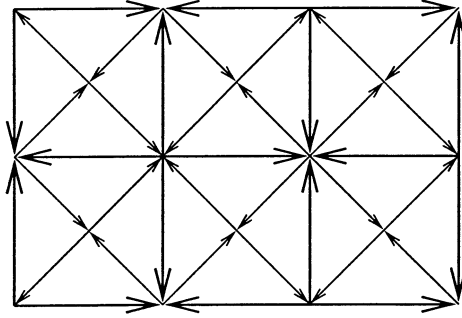
FIGURE 4. A choice of tangent vectors for the flat configuration of the Square-Diagonal lattice. The sum rule $\sum \vec{t} = \vec{0}$ is obeyed around each face.

of length $1/\sqrt{2}$. Let us fix a basic (flat) configuration of the long and short tangent vectors as in Fig.4, such that $\sum \vec{t} = \vec{0}$ around each face. A folding configuration is a length-preserving map ρ of the tangent vectors preserving the faces. Note that long vectors are mapped to long vectors.

Actually, the images of the long tangent vectors may only take either of the four values $\pm \vec{e}_i$, $i = 1, 2$, where $\vec{e}_i$, $i = 1, 2$ is the canonical basis of $\mathbb{R}^2$. The folding state of the lattice is almost entirely specified by the images of these long tangent vectors. More precisely, we have listed in Fig.5 the various possible arrangements of long tangent vector images around a given square face of the lattice with long edges. Here $e \in \{\pm \vec{e}_i\}$ may take 4 values, and $f \perp e$ the two other values perpendicular to e. The weight 2 affected to the first configuration is due to the existence of two possible inner tangent vector configurations compatible with the long one. Indeed, if $e = \vec{e}_1$ and $f = \vec{e}_2$ for instance, then the short edges of an inner triangular face must have images $(-(e+f)/2, (f-e)/2)$ or vice versa, which gives two distinct configurations. This gives rise to 28 distinct configurations of the long edge vectors around a square face.

We may now rephrase the folding problem into a coloring problem, by attaching a color $i = 1, 2$ to each long tangent vector with image $\pm \vec{e}_i$. Let us also consider the square lattice dual to that of long edges in the initial Square-Diagonal lattice. We can view the above face model as a dual vertex model with the allowed configurations of Fig.5, in which the edges of the square lattice are colored with colors 1 or 2. Once the color i of a long edge is specified, we still need to specify the sign $\epsilon = \pm 1$ determining the tangent vector $\epsilon \vec{e}_i$. Looking at Fig.5, we see that the sign is the same on all edges in the first configuration, the same on all edges of the same color in the second and third, and is flipped at the crossing with a line of opposite color in the fourth. This means that the value of the sign ϵ on an edge determines that on the whole cluster of same color connected to it. We therefore need to introduce an extra weight of 2 per colored cluster. Note that, independently, the first vertex still receives a weight 2.

The total number of folding configurations of the Square-Diagonal lattice therefore reduces to the sum over colored edge clusters on the square lattice (with two

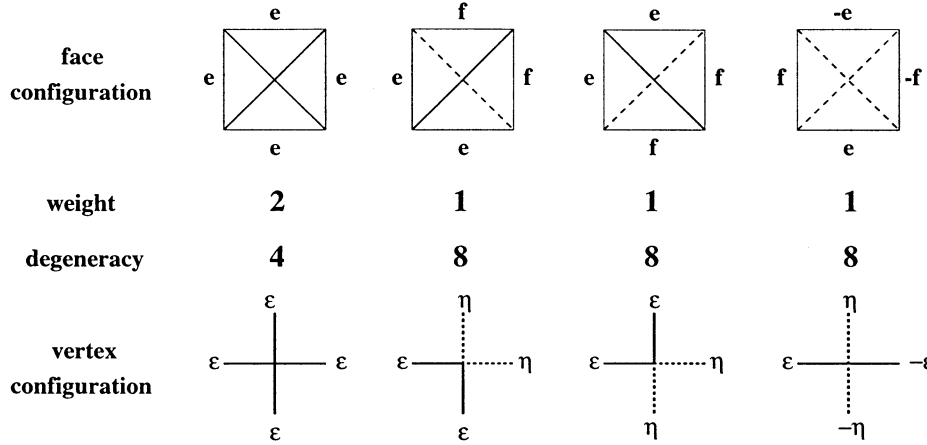|				
face configuration	e / e □ e / e	f / e ⊠ f / e	e / e ⊠ f / f	-e / f ⊠ -f / e
weight	2	1	1	1
degeneracy	4	8	8	8
vertex configuration	ε — ε — ε / ε	η ⋯ ε — η / ε	ε — ε — η / η	η ⋯ ε — −ε / −η

FIGURE 5. The 28 possible configurations of long tangent vectors around a large square face. We have $e \perp f$. We have indicated by short solid (resp. dashed) lines the folded (unfolded) inner short edges. We have also listed the weights attached to each configuration: the weight 2 for the first one corresponds to the two possible choices of inner short tangent vectors compatible with the sum rule (2.9). The degeneracy, i.e. the number of distinct configurations, is also indicated, leading to a total of 28 face configurations. In the last line, we have represented the dual vertices, with colors $1, 2$ in solid and dashed lines, and the signs $\pm\epsilon$, $\pm\eta$ of the corresponding tangent vectors.

colors $i = 1, 2$)

$$(2.11) \qquad\qquad Z_{\text{SD}} = \sum_{\text{colored clusters}} 2^{\#\text{ clusters}} \, 2^{\#\text{ 4-crossings}}$$

where each cluster receives a factor 2 and each "four-crossing" of edges of same color receives a weight 2.

The formulations as face or vertex model allow for many exact bounds and a numerical study of the entropy of folding, estimated as $s_{\text{SD}} \simeq .2299....$ In the next section, we give yet another formulation of the model as a gas of fully-packed loops, very similar to a well-known integrable model.

2.6. Fully-Packed Loops, Temperley-Lieb Algebra and Square-Diagonal Folding.
Let us again look at the folding configurations of the Square-Diagonal lattice, but this time let us concentrate on the images of the four short edges inside each large square face. The images of the short edges determine the folding state of the membrane completely, through (2.9). But these are still constrained as follows. Let us introduce the basis $\vec{f}_1 = (\vec{e}_1 + \vec{e}_2)/\sqrt{2}$, $\vec{f}_2 = (\vec{e}_2 - \vec{e}_1)/\sqrt{2}$ of $\mathbb{R}^2$.

(i) the two short edge vectors around each face must be perpendicular, i.e., one of them is equal to $\pm\vec{f}_1$ and the other to $\pm\vec{f}_2$.

(ii) any two adjacent triangular faces sharing a long edge have short edges with either of the two possible images below corresponding respectively to an unfolded or folded long edge.

(2.12)

Each of the short edges has an image tangent vector of the form $\epsilon \vec{f_i}$, with $\epsilon = \pm 1$. Let us again associate the color i ($\in \{1,2\}$) to such an edge. According to (ii), there are two possible coloring configurations of the short edge vectors on two triangles sharing a long edge. Instead of representing the painted short edges, let us represent their duals in the dual of the square lattice formed by the short edges, using solid lines for color 1 and dashed lines for color 2. At a joint between two triangles sharing a long edge, the two possibilities of (ii) (2.12) translate into

(2.13)   or

or the same pictures with the colors interchanged. This takes care of the colors, but we also have to specify the sign ϵ in $\vec{t} = \epsilon \vec{f_i}$. From (2.12), it is clear that this sign propagates along edges of the same color.

So finally, the folding problem of the Square-Diagonal lattice may be rephrased as a model of loops of two colors, obtained by covering the faces of the long edge lattice (denoted by S) by either of the two configurations

(2.14)   or

and by attaching a weight 2 per loop of a given color (accounting for the two choices of signs along that loop). We prefer the terminology "loops", rather than "lines", but this depends on the boundary conditions we impose to our portion of $P \times Q$ lattice faces. If we impose periodic boundary conditions, by identifying the right and left long edges on one hand and the top and bottom long edges on the other, the solid and dashed lines indeed form loops on the torus. Moreover, these loops are called *fully-packed*, as each middle of the edges of the original faces is visited by one loop of each color. The bulk result about the thermodynamic entropy should not depend on boundary conditions, so this choice is licit. With these choices, the counting function (2.11) becomes

(2.15)
$$Z_{\mathrm{SD}} = \sum_{\substack{\text{coverings of } S \\ \text{with } \square \text{ or } \square}} 2^{N_1 + N_2}$$

where N_i denotes the number of loops of color i in a given coloring configuration. This new expression (2.15) gives access to more exact bounds on the thermodynamic folding entropy.

Here we will rather concentrate on the algebraic structure underlying this model. Let us slightly generalize the model (2.15) by replacing the factors of 2 by a factor β_i per loop of color i. This leads to a "partition function" $Z_{\mathrm{SD}}(\beta_1, \beta_2)$. This is actually a two-color generalization of the Dense Loop model, defined as the same model, without the edges of color 2, namely with partition function

$$(2.16) \qquad Z_{\mathrm{DL}}(\beta) \;=\; \sum_{\substack{\text{coverings of } S \\ \text{with } \square \text{ or } \square}} \beta^L$$

where L denotes the total number of loops formed by the edges of color 1. This model plays a very important role as a sort of archetype of two-dimensional integrable lattice model, due to its underlying Temperley-Lieb algebra structure.

Let us now give the pictorial representation of the Temperley-Lieb algebra $TL_n(\beta)$, made of simple dominos and their linear combinations. By domino, we mean a rectangle with a top and bottom row of points labelled 1, 2, ..., n, and pairwise connected among themselves through n non-intersecting curves. Two dominos d_1 and d_2 are multiplied by concatenation (by putting d_1 on top of d_2), and by identifying the bottom points of d_1 with the top points of d_2. Whenever a contractible loop is formed inside a domino, we may erase it and replace it by a factor β. The algebra $TL_n(\beta)$ is the extension of the set of dominos by linear combinations. The algebra is generated by the identity domino, connecting the upper and lower points by vertical lines, and by

$$(2.17) \qquad e_i =$$

for $i = 1, 2, ..., n-1$. To make contact with the Fully-Packed Loop model above, let us represent the part of e_i not acting like the identity as a square "face" operator

$$(2.18) \qquad e_i =$$

$$= \; 1 \otimes 1 \otimes \cdots \otimes 1 \otimes e \otimes 1 \otimes 1 \otimes \cdots \otimes 1$$

where the face operator e acts on the i-th and $(i+1)$-th lines, by connecting them. The definition (2.18) makes transparent the following algebraic relations satisfied by the e_i's

FIGURE 6. The first and second relation of (2.19).

$$
\begin{aligned}
e_i^2 &= \beta \, e_i \\
e_i e_{i\pm1} e_i &= e_i \\
e_i e_j &= e_j e_i \quad \text{for } |i-j| > 1
\end{aligned}
$$
(2.19)

easily checked pictorially.

The first relation in (2.19) is consistent with the weight β per loop in (2.16): as shown in Fig.6, we can erase the loop formed by e_i^2 and replace it by a factor β. The second relation expresses that one can "pull" the black lines, as illustrated in Fig.6. The last relation simply expresses the locality of the action of the face operator at lines i and $i+1$.

To write the partition function of the dense loop model, we introduce a diagonal zigzag-to-zigzag transfer matrix

$$
\begin{aligned}
T_\beta &= U_\beta \, V_\beta \\
U_\beta &= \prod_{i=1}^{P-1} (1 + e_{2i}) \\
V_\beta &= \prod_{i=1}^{P} (1 + e_{2i-1})
\end{aligned}
$$
(2.20)

The partition function of the model on a strip of width $2P$ and height $2M$, counted in numbers of lines (with $N = 4PM$, as the total number of faces of S is $N/4 = PM$), with periodic conditions along its width $2P$ boundaries reads

$$
Z_{\,\mathrm{DL}}(\beta) = \mathrm{Tr}(T^M)
$$
(2.21)

where the trace is the standard trace on the Temperley-Lieb algebra $TL_{2P}(\beta)$, defined recursively by $\mathrm{Tr}(1) = \beta^{2P}$ and the recursion relation (Markov property)

$$
\mathrm{Tr}\big(e_{i+1} E(e_1, e_2, ..., e_i)\big) = \frac{1}{\beta} \, \mathrm{Tr}\big(E(e_1, e_2, ..., e_i)\big)
$$
(2.22)

for any expression E depending on the e_k, $k \leq i$ only. With this definition, (2.21) is calculated by simply first expanding T^M as a sum of products of e's and 1's, each corresponding to one covering of the faces of S (now tilted by 45°) with either

(2.23) $\leftrightarrow e$ or $\leftrightarrow 1$

Then we identify the top and bottom of the lines along the horizontal zigzag boundaries, and replace each loop by a factor of β, thus realizing exactly the sum in (2.16).

The abstract definition (2.19) of the algebra of the e's makes it possible to calculate (2.21) by choosing a particular representation for the algebra. A particular choice relates it to the partition function of the 6 Vertex model [15], solved with standard Bethe Ansatz techniques. This gives an exact formula for the thermodynamic entropy per site of the dense loop model [15]

$$(2.24) \qquad s_\beta \;=\; \begin{cases} \int_{-\infty}^{\infty} \frac{\sinh(\pi-\mu)x \;\; \tanh \mu x}{2x \;\; \sinh \pi x} & \text{for } \;\; \beta = 2\cos\mu, \;\; 0 < \mu < \pi \\ \frac{\lambda}{2} + \sum_{n=1}^{\infty} \frac{e^{-n\lambda}}{n} \tanh n\lambda & \text{for } \;\; \beta = 2\cosh\lambda, \;\; \lambda > 0 \\ 2 \; \text{Log} \; \frac{\Gamma(\frac{1}{4})}{2\Gamma(\frac{3}{4})} & \text{for } \;\; \beta = 2. \end{cases}$$

This takes care of all the values of $\beta \geq 0$. The value $\beta = 2$ is critical, as it lies at the transition between two regimes. Note that there are $N/4$ sites in the model, as there are 4 triangles of the original square-diagonal lattice on each face of S. The entropies *per triangle* are therefore those of (2.24) divided by 4.

The exact solvability of this Dense Loop model can be understood as follows. Defining $W_i(x) = 1 + xe_i$, we check that the Yang-Baxter equation

$$(2.25) \qquad W_i(x)W_{i+1}(xy)W_i(y) \;=\; W_{i+1}(y)W_i(xy)W_{i+1}(x)$$

is satisfied, as an immediate consequence of the relations (2.19), if and only if $a(x) = (x-1)/(z - x/z)$ for any solution z of $z + 1/z = \beta$ and up to any rescaling $x \to x^\gamma$, $\gamma \in \mathbb{R}$ (note that this includes the "rational" limit $x = e^{\epsilon u}$, $z = e^{\frac{\epsilon}{2}}$, $\epsilon \to 0$; hence $\beta = 2$ and $a(x) \to r(u) = u/(1-u)$). We also have the normalization condition $W_i(x)W_i(1/x) = I$. These two relations ensure the existence of a one-parameter family of commuting transfer matrices $T(x)$, with $[T(x), T(y)] = 0$. This justifies the existence of a common basis of eigenvectors for these, independent of x. That a Bethe Ansatz should yield them is not guaranteed, although it seems to be the case in all the known situations. In the present case, it may be viewed as a consequence of matrix functional relations satisfied by T (algebraic Bethe Ansatz).

Going back to the loop formulation of the Square-Diagonal folding problem, namely the Bi-Colored Fully-Packed-Loop model with partition function $Z_{\text{SD}}(\beta_1, \beta_2)$, we can express the transfer matrix of the model in terms of *two* Temperley-Lieb algebras, one for each color of loop. Tilting the lattice S by 45 degrees, we are led to the introduction of the following face operators:

$$e_i \;=\;$$

$$= (1 \otimes 1) \otimes ... \otimes (1 \otimes 1) \otimes (e \otimes 1) \otimes (1 \otimes 1)...(1 \otimes 1)$$

(2.26)

$$f_i \;=\;$$

$$= (1 \otimes 1) \otimes ... \otimes (1 \otimes 1) \otimes (1 \otimes e) \otimes (1 \otimes 1)...(1 \otimes 1)$$

acting on a set of $2P$ pairs of parallel lines of color 1 and 2 (in each parenthesis of (2.26), the first term of the tensor product corresponds to the color 1 and the

second to the color 2; note also that by a slight abuse of notation $1 \otimes e$ really means $(1 \otimes 1) \otimes e$, acting on the two pairs of consecutive lines of position i and $i+1$ of respective colors 1 and 2).

We see that the operators e_i and f_i satisfy the relations (2.19) for respectively $TL_{2P}(\beta_1)$ and $TL_{2P}(\beta_2)$, whereas $[e_i, f_j] = 0$ for all i, j. We can now define the zigzag-to-zigzag transfer matrix

$$
\begin{aligned}
T &= U \ V \\
(2.27) \qquad U &= \prod_{i=1}^{P}(e_{2i} + f_{2i}) \\
V &= \prod_{i=1}^{P}(e_{2i-1} + f_{2i-1}).
\end{aligned}
$$

The partition function for a portion of size $2P \times 2M$ of the square-diagonal lattice on a cylinder can be finally expressed as

$$(2.28) \qquad\qquad Z_{\text{SD}}(\beta_1, \beta_2) = \text{Tr}(T^M)$$

by imposing periodic conditions along the horizontal zigzag boundaries. In (2.28), the trace is defined for a tensor product of any two elements $E \in TL_{2P}(\beta_1)$ and $F \in TL_{2P}(\beta_2)$ as $\text{Tr}(E \otimes F) = \text{Tr}(E)\,\text{Tr}(F)$, and extended by linearity.

The above remark about the independence of $Z_{\text{DL}}(\beta)$ on the particular representation chosen for e_i is still valid here, and extends to the choice of representation for f_i as well. This would enable us for instance to map the model onto a pair of coupled 6 Vertex models (the 28 vertex model of the previous section is an example of such a mapping).

The analogy with the Dense Loop model however stops here, as we have not been able to find a one-parameter family of commuting transfer matrices for the Square-Diagonal folding problem. It is nevertheless a remarkable fact that its underlying algebraic structure consists of two copies of the Temperley-Lieb algebra, with both critical parameters $\beta_1 = \beta_2 = 2$. However, the model can still be studied in the continuum thermodynamic limit, where we take simultaneously the lattice spacing to zero while the dimensions of the piece of lattice M, N tend to infinity. It can then be shown to be described by a conformal field theory with central charge $c = 2$, for the folding problem $\beta_1 = \beta_2 = 2$, and more generally $c = 2 - 6\big(e_1^2/(1 - e_1) + e_2^2/(1 - e_2)\big)$ for $\beta_i = 2\cos\pi e_i$.

2.7. Folding of the Double-Triangular Lattice. The double-triangular lattice of Fig. 2 has three types of edges: long, medium, and short of respective lengths 2, $\sqrt{3}$, and 1. Each triangular face has one edge of each type. As usual, we introduce tangent vectors along these edges, with compatible orientations throughout the lattice, so that the face rule (2.8) is satisfied around each triangular face.

A folding configuration of the lattice is a continuous map ρ of these tangent vectors to the plane, such that the face rule (2.9) is satisfied around each elementary triangular face. Let us now first concentrate on the long edges of the double-triangular lattice. They form the Diamond lattice, represented in solid lines in Fig. 7, which is dual to the Kagomé lattice, represented in dashed lines in the same figure.

By inspection, it is easy to see that the images of the long edge vectors may take only one of the six values $\pm\vec{e_1}$, $\pm\vec{e_2}$, $\pm\vec{e_3}$, where the $\vec{e_i}$ are three fixed vectors
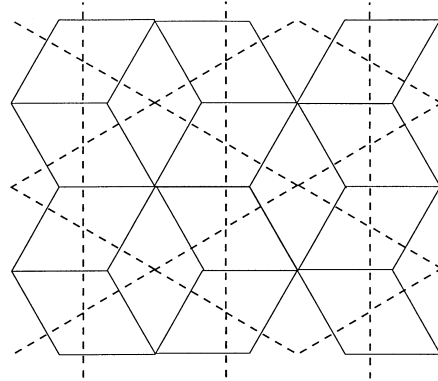
FIGURE 7. The diamond lattice formed by the long edges of the double-triangular lattice (solid lines) and its dual, the Kagomé lattice (dashed lines).

of length 2 with vanishing sum (hence forming angles of 120°). As before, writing these images as

$$(2.29) \qquad\qquad \rho(\vec{t}) \;=\; \epsilon \vec{e_i}$$

suggests attaching a color $i = 1, 2, 3$ to each long edge, and a sign $\epsilon = \pm 1$.

In a way very similar to the square-diagonal case, the long edges around any diamond-shaped face of Fig. 7 may take only the four possible relative values depicted in Fig. 8, according to the folding state of the inner short and medium edges. Note the weights: 1 for the last three cases of Fig. 8, as the inner edges are entirely fixed, and 2 for the first case, as we have two choices for the inner short edges $\vec{s} = \epsilon \vec{e_k}/2$, $k \neq i$, which then fix all other inner edges. Each long edge may take 6 values. This gives a total of 78 distinct possible diamond face environments.

We may now rephrase the folding problem as a Vertex model on the edges of the dual Kagomé lattice of Fig. 7, with the vertices derived from Fig. 8. Hence the model is equivalent to a colored cluster model with the vertices of Fig. 9, similar to that of the last line of Fig. 5, but this time with 3 edge colors, and with a weight 2 per vertex of the first type, and an extra weight of 2 per cluster of a given color.
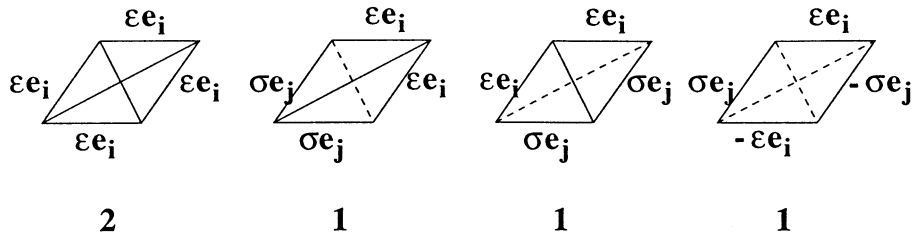
FIGURE 8. The four possible configurations of long edges around a diamond-shaped face. We have represented in dashed lines the (medium or short) unfolded inner edges, and in solid lines the folded inner edges. We have also indicated the attached weights. The color indices take the values $i, j = 1, 2, 3$, with $i \neq j$, and ϵ, σ are arbitrary signs.
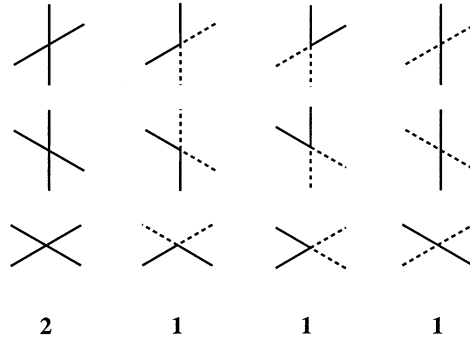
2   1   1   1

FIGURE 9. The allowed vertices of the tri-colored cluster model on the Kagomé lattice, equivalent to the two-dimensional DT folding problem. The solid and dashed lines stand for any two distinct colors among $\{1, 2, 3\}$. We have indicated the weight under the three corresponding vertices. Each colored cluster has an extra weight of 2, for the two choices of sign.

2.8. Higher Dimensional Folding. So far we have only discussed two-dimensional folding, by requiring that the image of the folding maps ρ be in $\mathbb{R}^2$. Relaxing this condition by considering higher-dimensional target spaces $\mathbb{R}^d$, $d > 2$, we obtain infinitely many possible maps, even on a finite subset S of the lattice we are folding. However, we would like to still deal with discrete models, having finitely many folding configurations for finite S. This can be obtained by restricting the image of the membrane under a folding map to be a subset of a d-dimensional lattice, compatible with the membrane structure. Again, we view the target lattice as a regular graph, i.e. as a set of vertices connected by edges.

By compatible, we mean that the target d-dimensional lattice contains the 2-dimensional lattice we are folding, and allows for folding configurations which are truly d-dimensional (and not included in a space of lesser dimension). Let us describe the target lattices we know to be compatible with the square, triangular, square-diagonal and double-triangular membranes of Fig. 2.

Square Lattice: The target is the d-dimensional hyper-cubic lattice (HC on Fig. 10), but the model is still easily seen to have a vanishing thermodynamic entropy. Indeed, if an edge is folded by a certain (right or flat) angle, then the whole line it belongs to is folded. So the number of folding configurations of a rectangle of $P \times Q$ faces is certainly less than $\left(2(d-1)\right)^{P+Q-2}$; hence the limit (2.2) vanishes.

Triangular Lattice: The target is the d-dimensional Face Centered Cubic lattice (FCC on Fig. 10) defined as follows. We start from the basis $\vec{f}_i = \vec{e}_i/\sqrt{2}$, $i = 1, 2, ..., d$ of $\mathbb{R}^d$, expressed in terms of the canonical basis. We then form the unit cell of our lattice by joining the vertices at $\pm\vec{f}_i$ with edges along the unit vectors $\pm\vec{f}_j \pm \vec{f}_k$: the result is the d-dimensional generalization of an octahedron (for $d = 3$), with $2d$ vertices, $2d(d-1)$ edges and $4d(d-1)(d-2)/3$ equilateral triangular faces of unit edge. The lattice is then generated by translation of this cell by integer multiples of the vectors $\pm\vec{f}_j \pm \vec{f}_k$. As we have increased the possibilities
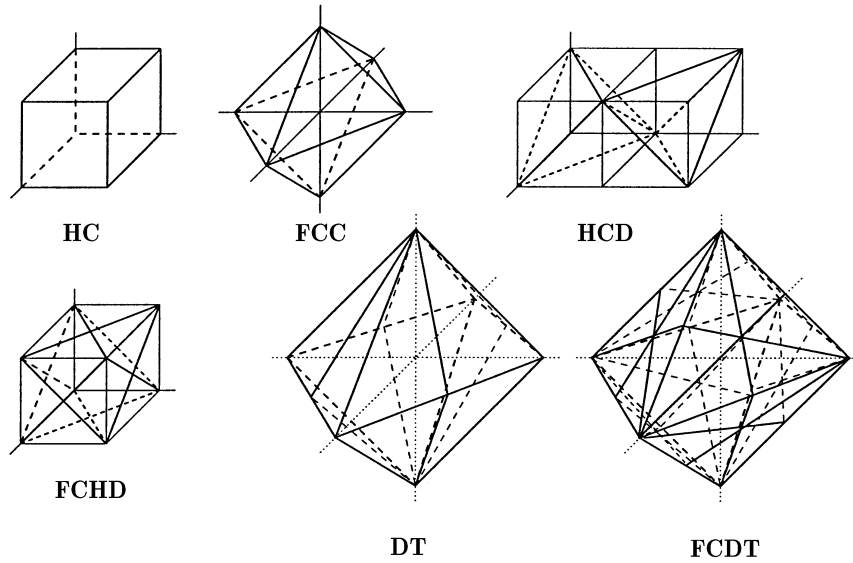
FIGURE 10. The d-dimensional lattices compatible with the folding of the membranes of Fig.2 are represented for $d = 3$. They are the Hyper-Cubic lattice (HC) compatible with the square lattice; the Face-Centered Cubic lattice (FCC), compatible with the triangular lattice; the Hyper-Cubic Diagonal (HCD) and Face-Centered-Hypercubic-Diagonal (FCHD), both compatible with the Square-Diagonal lattice; the Double-Triangular (DT) and the Face-Centered-Double-Triangular (FCDT), both compatible with the Double Triangular lattice.

of folding of the two-dimensional membrane, the entropy has increased and is still non-zero.

As usual we choose the orientations of the tangent vectors on both the membrane and the target so as to satisfy (2.8). A folding configuration is a map ρ from the membrane to the target tangent vectors satisfying (2.9). The images of tangent vectors around a triangular face of the membrane must take values of the form

(2.30)

with i, j, k all distinct, and $\epsilon, \sigma, \tau = \pm 1$. Hence the d-dimensional FCC folding problem can be rephrased as a fully-packed (FP) colored loop model on the hexagonal lattice (dual to the membrane) with d colors $i = 1, 2, ..., d$, in which all edges are occupied by two loops of distinct colors. The signs of the corresponding components of the tangent vectors are completely fixed along each such loop by the value on one edge of the loop; hence this results in a weight 2 per colored loop (for the two choices of signs). Finally

$$(2.31) \qquad Z_{\text{d-FCC}} \; = \; \sum_{\substack{\text{FP colored loops}}} 2^{N_1 + N_2 + \dots + N_d}$$

where N_i denotes the total number of loops of color i in a given configuration. Notice the analogy between (2.31) and the two-dimensional Square-Diagonal folding partition function, except that (2.31) only makes sense for $d \geq 3$, for configurations like (2.30) to be allowed (with $i \neq j \neq k$).

Square-Diagonal Lattice: We have found two different candidates for the target, depending on whether the emphasis is put on long or short edges, namely the Hypercubic-Diagonal (HCD in Fig. 10) and the Face-Centered Hypercubic-Diagonal (FCHD in Fig. 10).

The HCD lattice is built by first forming a hypercubic lattice with unnormalized orthogonal basis $\vec{e}_1, ..., \vec{e}_d$ of edges of length $1/\sqrt{2}$ (short edges), and then drawing exactly one diagonal (long edge of unit length) on each of its square faces, in a consistent way so as to allow for non-trivial folding maps from the square-diagonal lattice to the d-dimensional HCD. Let us choose an orientation of the tangent vectors satisfying (2.8) on both the membrane and the target. A folding map ρ is entirely determined by the images of the short edge vectors, of the form $\rho(\vec{t}) = \epsilon \vec{e}_i$, $i = 1, 2, ..., d$, $\epsilon = \pm 1$. Let us assign a color $i = 1, 2, ..., d$ to such an image. As the two short edges of a triangle must remain orthogonal, the colors of their images must be distinct. Moreover, in this model, the long edges are either completely folded or not folded at all, as no intermediate angle is allowed by the target. Therefore we still have the only two possibilities (2.12) for the relative values of short edge vectors in two triangles sharing a long edge, except that now $\vec{u} = \epsilon \vec{e}_i$ and $\vec{v} = \sigma \vec{e}_j$, with $i \neq j$ and $\epsilon, \sigma = \pm 1$. Just like in (2.14), we may rephrase the model in the dual form as a loop model with colors $i = 1, 2, ..., d$, obtained by covering the faces of the long edge square lattice S by configurations of the form

(2.32)

where the dual edges are painted with colors distinct from that of their neighbors, when going clockwise around the face (namely $i \neq j$, $j \neq k$, $k \neq l$, $l \neq i$). It is easy to see that this gives rise to $d(d-1)(d^2 - 3d + 1)$ distinct coloring configurations like (2.32), but we must also fix the four signs of the edges, hence a total of $V_d = 16d(d-1)(d^2 - 3d + 1)$ edge configurations. Moreover, the transitions from a face to an adjacent one result only in the two possibilities of (2.13), but now with any two colors $i \neq j$ among $1, 2, ..., d$. The signs are easily seen to be completely determined along each colored loop by just one of them. We must therefore have a weight 2 per colored loop to account for the two choices of signs. With these rules, the partition function of the d-dimensional HCD folding problem reads

$$(2.33) \qquad Z_{\text{d-HCD}} \; = \; \sum_{\substack{\text{coverings of } S \\ \text{with } (2.32)}} 2^{N_1 + N_2 + \dots + N_d}$$

where N_i denotes the total number of loops of color i in a given coloring of the dual short edges in S.

The FCHD lattice is obtained by first building the hypercubic lattice with orthonormal basis $\vec{e}_i$, $i = 1, 2, ..., d$ of unit long edges, and then drawing the two diagonals on each square face, thus forming short edges of length $1/\sqrt{2}$. Let us choose an orientation of the tangent vectors satisfying (2.8) on both the membrane and the target, and let us concentrate on the images of the long tangent vectors to the membrane. Those take values of the form $\rho(\vec{t}) = \epsilon\vec{e}_i$, $i = 1, 2, ..., d$, $\epsilon = \pm 1$. The four images of long edge vectors around a face of S still take only the values of Fig. 5, but with $e = \epsilon\vec{e}_i$ and $f = \sigma\vec{e}_j$, with $i \neq j$, and the first configuration, where all four images are equal corresponds now to $2(d-1)$ possible configurations of inner short edges. Indeed, those may take any values of the form $(\pm\vec{e}_k - \epsilon\vec{e}_i)/\sqrt{2}$, where $k \neq i$, with alternating signs when we go around the face. Moreover, the degeneracies become respectively $2d$ for the first configuration and $4d(d-1)$ for each of the other three. This leads to a total of $W_d = 2d(6d-5)$ possible face configurations, hence in the dual picture to a W_d-Vertex model (c.f. the last line of Fig. 5), in which the dual of long edges are painted with a color $i = 1, 2, ..., d$, and signs propagate along clusters of given colors and are flipped at each crossing like in the fourth configuration of Fig. 5. This gives a factor of 2 per cluster, for the two choices of sign. In that last formulation, the partition function of the d-dimensional FCHD folding problem reads

$$(2.34) \qquad Z_{\text{d-FCHD}} = \sum_{\text{colored clusters}} 2^{N_1+N_2+...+N_d}(2(d-1))^C$$

where N_i denotes the total number of clusters of color i in a given cluster configuration, and C is the total number of "four-crossings" (i.e. when the four adjacent edges to a vertex have the same color).

Note that (2.33) is the natural d-dimensional generalization of (2.15), whereas (2.34) is the generalization of (2.11). That the two models coincide at $d = 2$ gives two distinct points of view, leading in particular to various bounds and estimates of the folding entropy [13]. We see also that for large d, the FCHD model is more economical, in that we only have to sum over W_d^{PQ} configurations to evaluate (2.34), to be compared with $V_d^{PQ} >> W_d^{PQ}$ in the HCD case (2.33).

Double-Triangular Lattice: We have found again two possible targets, the d-dimensional Double-Triangular lattice (DT in Fig. 10) and the d-dimensional Face-Centered Double-Triangular lattice (FCDT in Fig. 10).

The d-DT lattice is obtained from the d-FCC lattice by drawing exactly one height in each triangular face, in a consistent way so as to allow for non-trivial foldings. Note also that the d-FCC lattice must be dilated by a factor of 2 to ensure that the long edges have length 2, the medium $\sqrt{3}$ and the short 1. Let us attach tangent vectors to the edges of both the DT and the target d-DT lattices, subject to (2.8). A folding map ρ maps tangent vectors to tangent vectors, and satisfies (2.9) around each face. We may again visualize a folding configuration as a map on long and short tangent vectors. Indeed, medium edges can only be either completely folded or not folded at all. Moreover, a long edge image has the form $\rho(\vec{\ell}) = \epsilon\vec{e}_i + \sigma\vec{e}_j$, $1 \leq i \neq j \leq d$, where the $\vec{e}_i$'s form an orthogonal basis of $\mathbb{R}^d$, with lengths $\sqrt{2}$ and $\epsilon, \sigma = \pm 1$, and a short edge image has the form $\rho(\vec{s}) = (\epsilon\vec{e}_i + \sigma\vec{e}_j)/2$. This results in the following four possible long and short edge images around a diamond face of long edges. When the medium edges are flat, we

have

(2.35)

with $1 \leq i \neq j \neq k \leq d$ and $1 \leq j \neq k \neq m \leq d$ (m can be equal to i), and $\epsilon, \sigma, \tau, \eta = \pm 1$. When they are completely folded, we have

(2.36)

with the same restrictions.

This face model may be reformulated on the dual of the diamond lattice of long edges, namely the Kagomé lattice of Fig.7, as a colored cluster model, in the same spirit as Fig.9. Indeed, let us attach to each long edge image of the form $\rho(\vec{\ell}) = \epsilon \vec{e}_i + \sigma \vec{e}_j$ a pair of colors (ij), $1 \leq i \neq j \leq d$. We may now paint the duals of the long edges (i.e. the edges of the Kagomé lattice) with these pairs of colors: just think of each edge as two superposed lines, one of color i and one of color j. The allowed vertices are depicted in Fig.11, in correspondence with (2.35)-(2.36). The indicated weights correspond to the free choices of short and medium inner edge images, which are clear from (2.35)-(2.36). Moreover, each colored line i carries a sign (that in front of $\vec{e}_i$ in the corresponding image), which is preserved under a right or left turn, and flipped at the crossing with a line of different color. A simple counting argument leads to a total of $4d(d-1)(8d^2 - 36d + 41)$ possible vertices on each of the three subsets of vertices of the Kagomé lattice corresponding to different orientations of their adjacent edges.

To evaluate the partition function of the d-DT model, we must sum over all possible colored cluster configurations on the edges of the Kagomé lattice, allowed by Fig.11 and its two rotated versions under $\pm 120°$, including the extra weights indicated, and also with a weight 2 per cluster of a given color, to account for the two choices of signs. This gives

$$(2.37) \qquad Z_{\text{d-DT}} = \sum_{\text{colored clusters}} 2^{N_1 + N_2 + \ldots + N_d} (2(d-3))^a 4^b (4(d-2))^c$$

where N_i denote the numbers of clusters of color i in a given configuration, whereas a, b, c denote the numbers of vertices of the third, fourth and fifth type in Fig.11, as well as their rotated versions by $\pm 120°$.

The d-FCDT lattice is also made of the d-FCC lattice, on the triangular faces of which all three heights have been drawn, creating three inner short and long new
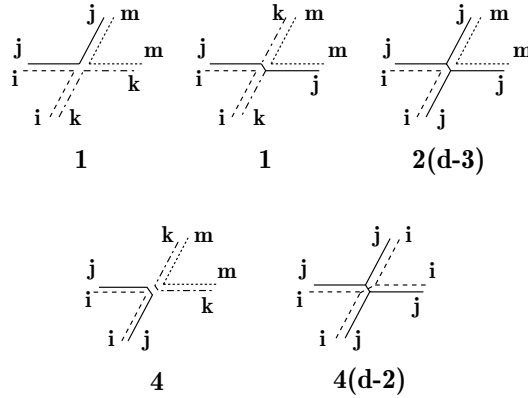
FIGURE 11. The Kagomé lattice colored cluster model dual to the d-DT model. The edges are colored with pairs (ij) of colors $1 \leq i \neq j \leq d$. In the first and second vertices, we have $1 \leq i \neq j \neq k \leq d$ and $1 \leq j \neq k \neq m \leq d$, and it is possible that $m = i$. In all the others the color indices are all distinct. Each colored line also carries a sign, which is preserved under a left or right turn, and flipped at a crossing with a line of different color. We have indicated the extra weights arising from the free choices of inner short and medium edge vectors.

edges, and cutting the edges of the d-FCC into two medium ones. Note that this time we must dilate the d-FCC lattice by a factor $2\sqrt{3}$ to ensure that long edges have length 2. Let us as usual choose tangent vectors subject to (2.8) on both the membrane and the target.

Denoting again by $\vec{e}_i$ an orthogonal basis of $\mathbb{R}^d$ with vectors of length $\sqrt{3/2}$, we may write the images of the medium edges under a folding map ρ as $\rho(\vec{m}) = \epsilon \vec{e}_i + \sigma \vec{e}_k$, with $\epsilon, \sigma = \pm 1$, and $1 \leq i \neq j \leq d$. Note that the short and long edges may only be either flat or completely folded, from the structure of the target. This therefore gives rise to the 11 possible arrangements of medium edges around each triangular face of the triangular lattice formed by the medium edges, depicted in Fig.12. Note that these 11 arrangements match the 11 vertices (2.4): they just represent the folding state of a face of the triangular lattice of medium edges of the membrane. The weight $4(d-1)$ for the last configuration is the number of possible triangles with one edge of each type and a specified medium image say $\rho(\vec{m}) = e = \epsilon \vec{e}_i + \sigma \vec{e}_j$. The long edge must have an image of the form $\rho(\vec{\ell}) = -2(2\epsilon \vec{e}_i + \sigma \vec{e}_j + \tau \vec{e}_k)/3$ or $-2(\epsilon \vec{e}_i + 2\sigma \vec{e}_j + \tau \vec{e}_k)/3$, with $1 \leq i \neq j \neq k \leq d$, and $\tau = \pm 1$, and the short edge image is then completely fixed by (2.9). These give twice $2(d-2)$, hence the total weight $4(d-2)$. A simple counting shows that there are $8d(d-1)(7d-13)$ distinct face configurations for the medium edge images, hence sensibly less than in the d-DT case. As before, the model could be rephrased as a colored cluster model with specific weights, but the corresponding expression for the partition function is not simple.

The various reformulations of the d-dimensional folding problems of this section give access to many analytic bounds for the thermodynamic folding entropies, and allow for numerical studies as well. It would be interesting to further study the algebraic structure of the corresponding vertex models. This remains to be done.

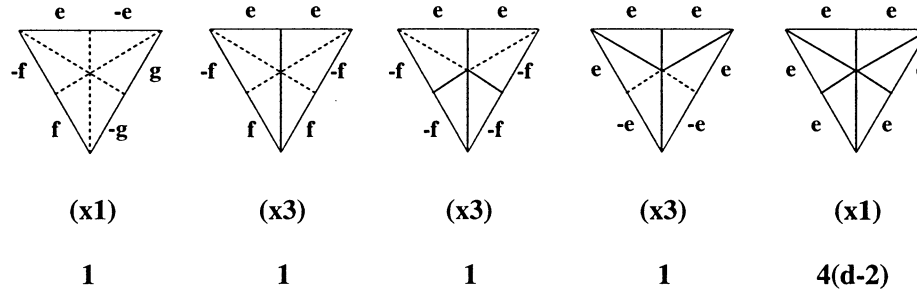| (x1)	(x3)	(x3)	(x3)	(x1)
1	1	1	1	4(d-2)

FIGURE 12. The eleven face configurations for medium edges in the d-FCDT model. The folded (resp. flat) short and long edges are represented in thick solid (resp. dashed) lines. The medium edge vectors take values e, f, g of the form $\epsilon \vec{e}_i + \sigma \vec{e}_j$, $1 \leq i \neq j \leq d$ and $\epsilon, \sigma = \pm 1$. We have $e + f + g = 0$ in the first configuration, and there exists a g of the same form, such that $e + f + g = 0$ in the next two. We have indicated the weight of each configuration, obtained as the number of possible short and long edge images compatible with the assignment of the medium ones.

3. FLUID MEMBRANE FOLDING: TRIANGULATIONS

Fluid membranes are modelled by irregular networks of vertices linked by edges, in which the valencies of the vertices are arbitrary, as well as the genus of the underlying surface, which might have an arbitrary topology. The study of such membranes is best performed within the context of random surfaces and two-dimensional quantum gravity (for a review, see [17] and references therein).

Two-dimensional quantum gravity can be viewed as the coupling between a two-dimensional system (say a two-dimensional lattice model, with its configurations and weights), and the fluctuations of space, namely by allowing the underlying lattice to fluctuate into irregular networks of arbitrary topology. A configuration of the system is then a particular choice of such a network, together with a configuration of the physical model defined on this particular network.

Hence we may view the folding problem of fluid membranes as the two-dimensional quantum-gravitational version of the folding problem of regular membranes.

3.1. Triangulations and Foldability. Now and in the following, we consider the toy model for fluid membranes, formed by arbitrary triangulations of surfaces of arbitrary topology, by means of equilateral triangles. The fluidity is rendered by the fact that any number of triangles may be adjacent to a vertex. In the spirit of the above, we are therefore dealing with the quantum-gravitational version of the triangular lattice.

We wish now to study the folding of such membranes, defined as before as continuous folding maps preserving the faces of the triangulations. To ensure the existence of interesting folding configurations, we will impose as in the lattice case that the membrane be foldable completely onto one of its faces, namely that there exist a folding map with image a single triangle. With this constraint, it is clear that not all triangulations turn out to be "foldable". Indeed, let us paint by three distinct colors $1, 2, 3$ the three vertices of the image triangle, and paint accordingly the vertices of the preimages under the folding map. This results in the tri-coloring

of the vertices of the initial triangulation, in such a way that the three colors around each triangular face are distinct. So only the vertex-tri-colorable triangulations will be foldable.

Another way of viewing this restriction is to recall that we first need to attach tangent vectors to the edges of the triangulation in such a way that (2.8) is satisfied. It is straightforward to see that this is possible only if the vertices of the triangulation are all even, as around such a vertex, we must have an alternance of tangent vectors pointing to and from it. This condition turns out to be sufficient in genus zero to grant the tri-colorability of the triangulation. The situation in higher genus is unclear [16].

In the next sections, we will introduce a generating function for tri-colorable triangulations in arbitrary genus. This will be done by use of a Hermitian multi-matrix integral, whose formal series expansion can be interpreted as a sum over tri-colorable triangulations. Let us state the main results before going into the detailed proofs. We will study the generating function

$$
\begin{aligned}
&f(x_1, x_2, x_3; t; N) \\
(3.1) \quad &= \sum_{\substack{\text{connected tricolorable} \\ \text{triangulations } T}} \frac{1}{|\operatorname{Aut}(T)|} N^{2-2g(T)} x_1^{v_1(T)} x_2^{v_2(T)} x_3^{v_3(T)} t^{\frac{A(T)}{2}}
\end{aligned}
$$

where the sum extends over all connected vertex-tricolorable triangulations, and $g(T), v_i(T), A(T)$ respectively stand for the genus, the total number of vertices of color i and the total number of faces (area) of the triangulation T. The division by the order of the symmetry group of the triangulation is standard and avoids overcounting. Introducing

$$
(3.2) \qquad Z(x_1, x_2, x_3; t; N) = e^{f(x_1, x_2, x_3; t; N)}
$$

we will express Z as an integral over Hermitian matrices, whose formal series expansion will be a sum over possibly disconnected triangulations. Our main result is the following

Theorem 3. *The partition function Z (3.2) satisfies the following discrete Hirota Bilinear equation*

$$
\begin{aligned}
(3.3) \quad &n\frac{t}{N} Z_{n+1}(a+1, b+1) Z_{n-1}(a, b) \\
&= Z_n(a+1, b+1) Z_n(a, b) - Z_n(a, b+1) Z_n(a+1, b)
\end{aligned}
$$

provided we define $a = Nx_1$, $b = Nx_2$, $n = Nx_3$ and $Z_n(a, b) \equiv Z(x_1, x_2, x_3; t; N)$.

We also have the following simple result for

$$
(3.4) \qquad f_0(x_1, x_2, x_3; t) = \lim_{N \to \infty} \frac{1}{N^2} f(x_1, x_2, x_3; t; N),
$$

the genus zero contribution to the generating function (3.1).

Theorem 4. *The generating function* $f_0(x_1, x_2, x_3; t)$ *for genus zero connected vertex-tricolored triangulations reads*

$$(3.5) \qquad\qquad t(t\partial_t)^2 f_0(x_1, x_2, x_3; t) = \prod_{i=1}^{3} F_i(x_1, x_2, x_3; t)$$

$$F_1(1 - F_2 - F_3) = tx_1$$

$$F_2(1 - F_3 - F_1) = tx_2$$

$$F_3(1 - F_1 - F_2) = tx_3$$

where $F_i(x_1, x_2, x_3; t) = tx_i + O(t^2)$ *are formal series of* t *with polynomial coefficients of the* x's.

3.2. Matrix Models and Graphs. Hermitian matrix integrals are a powerful tool to construct generating functions for random tessellations of Riemann surfaces of arbitrary topology (see [17] for a review). For any polynomial or formal series $V(x) = \frac{x^2}{2} + \sum_{i \geq 1} t_i \frac{x^i}{i}$, let us consider the following integral over $N \times N$ Hermitian matrices M

$$(3.6) \qquad\qquad Z(V; N) = \frac{1}{Z_0(N)} \int dM e^{-N \operatorname{Tr}(V(M))}$$

with the standard Haar measure $dM = \prod_{i<j} d\operatorname{Re} M_{ij} \, d\operatorname{Im} M_{ij} \prod_i dM_{ii}$, and a normalization factor $Z_0(N)$ such that $Z(V_0; N) = 1$, where $V_0(x) = \frac{x^2}{2}$. The integral (3.6) is understood only as a formal power series of the t_i's, the coefficients of which are well-defined Gaussian integrals. We will not be concerned with issues of convergence here.

To compute the integral (3.6), we therefore have to expand the t-dependent part of the exponential as a power series, and to compute the coefficient say of $\prod t_i^{v_i}$, of the form

$$(3.7) \qquad\qquad \frac{1}{Z_0(N)} \int dM e^{-N \operatorname{Tr}(\frac{M^2}{2})} N^{\Sigma v_i} \prod_i \frac{\operatorname{Tr}(M^i)^{v_i}}{i^{v_i} v_i!}.$$

Let us denote by $\langle f(M) \rangle = \int dM e^{-N \operatorname{Tr}(\frac{M^2}{2})} f(M)/Z_0(N)$ the Gaussian average of f. Note that $\langle M_{ij} \rangle = 0$ and that $\langle M_{ij} M_{kl} \rangle = \delta_{jk} \delta_{il}/N$. More generally, for any $N \times N$ Hermitian matrix S, we have

$$(3.8) \qquad\qquad \langle e^{\operatorname{Tr}(SM)} \rangle = e^{\frac{1}{2N} \operatorname{Tr}(S^2)}.$$
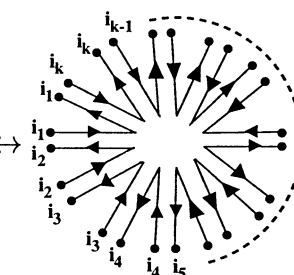
Therefore we deduce that

$$(3.9) \qquad \langle M_{i_1 i_2} M_{i_3 i_4} ... M_{i_{2k-1} i_{2k}} \rangle = \frac{\partial}{\partial S_{i_2 i_1}} \frac{\partial}{\partial S_{i_4 i_3}} ... \frac{\partial}{\partial S_{i_{2k} i_{2k-1}}} e^{\frac{1}{2N} \operatorname{Tr}(S^2)} \Bigg|_{S=0}.$$

To get a non-zero answer in (3.9), the derivatives wrt entries of S must be taken by pairs of the form $\partial_{S_{ij}} \partial_{S_{ji}}$, each of which extract a factor of $1/N$ from the exponential. Indeed, otherwise some single entry of S will be left in the end and will yield a zero result when we take $S = 0$. In particular, we will get a non-zero answer for (3.9) only if $k = 2p$ is even. This expresses the Wick theorem for Gaussian matrix integrals: the integral (3.9) is equal to the sum over all possible pairings of matrix elements

$$\langle M_{i_1 i_2} M_{i_3 i_4} ... M_{i_{4p-1} i_{4p}} \rangle = \sum_{\sigma \in S_{2p}} \frac{1}{N^p} \prod_j \delta_{i_{2j-1}, i_{2\sigma(j)}} \delta_{i_{2j}, i_{2\sigma(j)-1}}$$

(3.10)

$$= \sum_{\sigma \in S_{2p}} \prod_j \langle M_{i_{2j-1}, i_{2\sigma(j)}} M_{i_{2j}, i_{2\sigma(j)-1}} \rangle$$

where each matrix entry appears exactly once in each product. These pairings of matrix elements of M are called propagators. Let us use this result to evaluate the coefficients (3.7) of the expansion of Z. We must sum over all possible pairings of matrix elements of M. Let us represent this sum pictorially as follows. A matrix element of M will be represented by a double line with a marked end, such that the first line is oriented from and the second to the mark. These oriented lines carry a "color" index running from 1 to N, corresponding to the indices of the matrix entry. The main rule is that an index is constant along an oriented line. In this notation, the matrix element M_{ij}, propagator $\langle M_{ij} M_{kl} \rangle$ and product of matrix elements $M_{i_1 i_2} M_{i_2 i_3} ... M_{i_k i_1}$ leading to $\mathrm{Tr}(M^k)$ by summation over indices are represented respectively by half-edges, edges and vertices as follows

(3.11)

$$M_{ij} \leftrightarrow \quad , \quad \langle M_{ij} M_{kl} \rangle \leftrightarrow$$

$$\text{and } M_{i_1 i_2} M_{i_2 i_3} ... M_{i_k i_1} \leftrightarrow$$

Note that the index conservation rule implies that $i = l$ and $j = k$ in our representation of propagators: a propagator pairs up two marked double-ends corresponding to two matrix elements. The coefficient (3.7) is now obtained by summing over all ways of closing a set of v_i i-valent vertices ($i = 1, 2, 3..$) through propagators, thus creating a closed non-necessarily connected "fatgraph" or "ribbon graph" Γ whose edges are oriented double-lines. Each such graph contributes a factor $1/N^e$ to (3.7), where e denotes its total number of edges. The collection of weights associated to the vertices and edges of (3.11) are called "Feynmann rules" in physics. Moreover, the running indices must be summed over $\{1, 2, ..., N\}$, resulting in a factor N^L where L is the total number of loops of oriented lines, also equal to the number f of faces of the graph. Together with the factor $N^{\Sigma v_i} = N^v$, v the total number of vertices of the graph, this forms an overall factor of $N^{f-e+v} = N^{2-2g}$, where g denotes the genus of the graph. In addition, we are left with a product of $1/(i^{v_i} v_i!)$, to be summed over various labellings of the same graph, which leads to a factor $1/|\mathrm{Aut}(\Gamma)|$ for each graph Γ. We finally obtain

(3.12)
$$Z(V; N) = \sum_{\text{fatgraphs } \Gamma} \frac{1}{|\mathrm{Aut}(\Gamma)|} N^{2-2g(\Gamma)} \prod_i t_i^{v_i(\Gamma)}$$

where the sum extends over the non-necessarily connected fatgraphs, and $g(\Gamma)$, $v_i(\Gamma)$ denote respectively the genus and number of i-valent vertices of Γ. To transform the sum (3.12) into a sum over *connected* fatgraphs, we just have to take its

logarithm, as is immediately proved order by order in the formal series expansion.

This interpretation extends to multi-matrix integrals as well: if we denote by $Q_{\alpha,\beta}$ a symmetric $p \times p$ matrix, we may consider the integral over $N \times N$ Hermitian matrices M_1, M_2, ..., M_p:

$$(3.13) \quad Z(V_1, V_2, ..., V_p; Q; N) \;=\; \frac{1}{Z_0(Q; N)} \int dM_1 dM_2 ... dM_p e^{-N \operatorname{Tr}(V(M_1,...,M_p))}$$

where

$$(3.14) \qquad V(x_1, x_2, ..., x_p) \;=\; \sum_{\alpha,\beta=1}^{p} \frac{1}{2} x_\alpha Q_{\alpha,\beta} x_\beta + \sum_{\alpha=1}^{p} V_\alpha(x_\alpha)$$

for some arbitrary formal series $V_\alpha(x) = \sum_{i \geq 3} t_{i,\alpha} \frac{x^i}{i}$, and $Z_0(Q; N)$ is a normalization factor ensuring that $Z(0, 0, ..., 0; Q; N) = 1$. The reexpression (3.12) generalizes to

$$Z(V_1, V_2, ..., V_p; Q; N)$$

$$(3.15) \qquad = \sum_{\substack{\text{fatgraphs } \Gamma \text{ with} \\ p-\text{colored vertices}}} \frac{1}{|\operatorname{Aut}(\Gamma)|} \, N^{2-2g(\Gamma)} \prod_{i,\alpha} t_{i,\alpha}^{v_{i,\alpha}(\Gamma)} \prod_{\text{edges } e} Q_{\alpha(e),\beta(e)}^{-1}$$

where the sum extends over the non-necessarily connected fatgraphs Γ with vertices colored with colors $\alpha = 1, 2, ..., p$, and $g(\Gamma)$, $v_{i,\alpha}(\Gamma)$ and $\alpha(e), \beta(e)$ respectively denote the genus of Γ, the number of i-valent vertices of color α, and the colors of the two vertices linked by the edge e. The factors of $Q_{\alpha,\beta}^{-1}$ arise from the straightforward multi-Gaussian average (still denoted $\langle ... \rangle$) wrt the potential $V_0(x_1, ..., x_p) = \frac{1}{2} \sum_{\alpha,\beta} x_\alpha Q_{\alpha,\beta} x_\beta$:

$$(3.16) \qquad \langle e^{\operatorname{Tr}(\sum_\alpha S_\alpha M_\alpha)} \rangle \;=\; e^{\frac{1}{2N} \sum_{\alpha,\beta} \operatorname{Tr}(S_\alpha Q_{\alpha,\beta}^{-1} S_\beta)}$$

where S_α, $\alpha = 1, 2, ..., p$ are $N \times N$ Hermitian matrices. Note that in this picture the edges (propagators) of Γ are naturally bi-colored by the two colors of their adjacent vertices. As before, the sum over *connected* fatgraphs is simply obtained by taking the logarithm of (3.13).

The integral (3.13) gives access to a number of interesting combinatorial results on enumeration of colored graphs. In the following, we will see that a particular case of (3.13) with $p = 2$ matrices yields (upon taking the logarithm) the generating function (3.1).

What will we have gained in formulating our problem in terms of a matrix integral? It turns out that matrix integrals can be computed by alternative techniques using either orthogonal polynomials or discrete bilinear recursion relations or even a direct expansion method. By exploiting the two last approaches, we will be able to derive among others the results (3.3)(3.5).

3.3. A Generating Function for Tri-Colored Triangulations.

Our main result will be based on the following matrix representation for $Z(x_1, x_2, x_3; t; N)$ of (3.2) (3.1). Let us consider the double integral over $n \times n$ Hermitian matrices M_1 and M_2

$$(3.17) \qquad Z_n(x_1, x_2; u; N) \;=\; \frac{1}{\varphi_n(u, N)} \int dM_1 dM_2 e^{-N \operatorname{Tr} V(M_1, M_2; x_1, x_2, u)}$$

$$V(M_1, M_2; x_1, x_2, u) \;=\; x_1 \operatorname{Log}(1 - M_1) + x_2 \operatorname{Log}(1 - M_2) + u M_1 M_2$$

where the logarithms are understood as the corresponding formal series expansions $- \operatorname{Log}(1-x) = \sum_{n \geq 1} x^n / n$, and the prefactor $\varphi_n(u, N)$ ensures that $Z_n(0, 0; u; N)$ $= 1$. Note that here N can be any real number, unrelated to n, the size of the matrices. Note also that (3.17) has the form (3.13) up to the change $n \to N$, and that the quadratic form is just reduced to $Q_{1,2} = Q_{2,1} = u$, $Q_{1,1} = Q_{2,2} = 0$. For (3.17) to make sense, we must give a prescription for computing the (a priori ill-defined) "Gaussian" average

$$\langle f(M_1, M_2) \rangle = (1 / \varphi_n(u, N)) \int dM_1 dM_2 f(M_1, M_2) e^{-Nu \operatorname{Tr}(M_1 M_2)}.$$

We choose to define it by use of Feynmann rules derived from those for (3.11), namely by the two-dimensional formal integral

$$(3.18) \qquad \langle x^\alpha y^\beta \rangle = Nu \int dx dy e^{-Nuxy} x^\alpha y^\beta = \Gamma(\alpha + 1)(Nu)^{-\alpha} \delta_{\alpha, \beta}$$

for any real α, β (we have identified $\varphi_1(u, N) = 1/(uN)$).

This induces the propagator $\langle (M_1)_{ij}(M_2)_{kl} \rangle = \delta_{il} \delta_{jk} / (Nu)$. Following the steps leading to (3.15), we see that $Z_n(x_1, x_2; u; N)$ generates a sum over non-necessarily connected vertex-bicolored graphs Γ (color 1 for M_1 and 2 for M_2), such that adjacent vertices have distinct colors (there are only edges coming from propagators $\langle M_1 M_2 \rangle$), with a weight $1/(Nu)$ per edge (the inverse of the quadratic form is just $1/u^2$ times itself), and a weight Nx_1 per vertex of color 1 and Nx_2 per vertex of color 2. Note that now the loops of the graph have running indices $i = 1, 2, ..., n$; hence give a contribution n^f to each graph with f faces. Writing $n = Nx_3$, this becomes $N^f x_3^f$. The factors of N therefore conspire to yield the usual $N^{2-2g(\Gamma)}$, and we are left with

(3.19)

$$Z_n(x_1, x_2; u; N) = \sum_{\substack{\text{vertex-bicolored} \\ \text{fatgraphs } \Gamma}} \frac{1}{|\operatorname{Aut}(\Gamma)|} N^{2-2g(\Gamma)} x_1^{n_1(\Gamma)} x_2^{n_2(\Gamma)} x_3^{f(\Gamma)} u^{-e(\Gamma)}$$

where $n_i(\Gamma)$ is the number of vertices of color i in Γ, $f(\Gamma)$ the number of faces of Γ and $e(\Gamma)$ the total number of edges of Γ.

How can we use this for tricolored triangulations? Starting from a vertex-bicolored fatgraph Γ involved in (3.19), let us create a new vertex, say of color 3, in the middle of each of its faces, and connect it to all the surrounding vertices by means of new edges. The result is a vertex-tricolored triangulation T, as each triangular face is adjacent to one vertex of each color 1, 2 and 3. Conversely, any vertex-tricolored triangulation gives rise to a vertex-bicolored fatgraph by simply erasing the vertices of color 3. Note that the number of edges in the original bicolored fatgraph Γ is equal to $A(T)/2$, where $A(T)$ is the number of triangular faces of T, as an edge linking vertices of colors 1 and 2 is adjacent to two triangles in T. It is a simple exercise to check that the symmetry group is preserved from Γ to T; hence finally upon setting

$$(3.20) \qquad\qquad t = \frac{1}{u} \qquad \text{and} \qquad x_3 = \frac{n}{N}$$

we have the identity

$$Z_n(x_1, x_2; u; N) = Z(x_1, x_2, x_3; t; N)$$

$$(3.21) \qquad = \sum_{\substack{\text{tricolorable} \\ \text{triangulations } T}} \frac{1}{|\operatorname{Aut}(T)|} N^{2-2g(T)} x_1^{v_1(T)} x_2^{v_2(T)} x_3^{v_3(T)} t^{\frac{A(T)}{2}}.$$

This identification is actually valid only as that between two formal series of $t = 1/u$, namely between their coefficients, which are polynomials of $(x_1, x_2, \frac{n}{N} = x_3)$. Although n and N only take integer values in the identification, as we only need a finite number of distinct values to completely specify a polynomial, the analytic continuation to arbitrary real or complex x_3 is immediate.

We may now study the two-matrix integral (3.17).

3.4. Discrete Hirota Equation.
A crucial step towards the complete determination of (3.17) is the reduction to integrals over the eigenvalues of M_1 and M_2. This involves the change of variables $M_i \to (U_i, m_i)$ where $M_i = U_i m_i U_i^\dagger$, U_i unitary and m_i diagonal $n \times n$ matrices. The Haar measure is known to transform with the Jacobian $J(m_1, m_2) = \Delta(m_1)^2 \Delta(m_2)^2$, where $\Delta(a) = \prod_{1 \le i < j \le n}(a_i - a_j)$ is the Vandermonde determinant of the diagonal matrix a. Moreover the only non-invariant term under unitary conjugation of M_1 and M_2 is the crossed term $\operatorname{Tr}(M_1 M_2)$. We therefore have

$$Z_n(x_1, x_2; u; N) = \frac{1}{\phi_n(u, N)} \int dm_1 dm_2 \Delta(m_1)^2 \Delta(m_2)^2$$

$$(3.22) \qquad \times e^{-N \operatorname{Tr}(x_1 \operatorname{Log}(I-m_1) + x_2 \operatorname{Log}(I-m_2))} \int dU_1 dU_2 e^{-Nu \operatorname{Tr}(U_2^\dagger U_1 m_1 U_1^\dagger U_2 m_2)}$$

where the normalization $\phi_n(u, N)$ ensures that $Z_n(0, 0; u; N) = 1$. Introducing the unitary matrix $\Omega = U_1^\dagger U_2$, we may compute the second integral, which up to an overall factor depending only on n reads

$$(3.23) \qquad \int d\Omega e^{-Nu \operatorname{Tr}(\Omega^\dagger m_1 \Omega m_2)} \propto \frac{1}{\Delta(m_1)\Delta(m_2)} \det \left(e^{-Num_{1,i}m_{2,j}}\right)_{1 \le i,j \le n}$$

where the integral extends over the unitary group $U(n)$, and $m_{i,k}$ is the k-th eigenvalue of M_i. This is the Itzykson-Zuber formula [21], a particular case of the Harish Chandra and Duistermaat-Heckmann localization formulas [22]. An elementary proof was given in [21], using the matrix Heat equation. Using the skew-symmetry of the determinants, this leads to

$$(3.24)$$

$$Z_n(x_1, x_2; u; N) = \frac{1}{\psi_n(u, N)} \int dm_1 dm_2 \Delta(m_1)\Delta(m_2) e^{-N \operatorname{Tr}(V(m_1, m_2; x_1, x_2, u))}$$

where the normalization factor $\psi_n(u, n)$ ensures that $Z_n(0, 0; u; N) = 1$. It is easily derived by expanding the two determinants as sums over permutations, with the

result

$$\psi_n(u, n) = \int dm_1 dm_2 \Delta(m_1) \Delta(m_2) e^{-Nu\,\mathrm{Tr}(m_1 m_2)}$$

$$(3.25) \qquad = \sum_{\sigma, \tau \in S_n} \mathrm{sgn}(\sigma\tau) \prod_{i=1}^{n} \int dm_{1,i} dm_{2,i} m_{1,i}^{\sigma(i)-1} m_{2,i}^{\tau(i)-1} e^{-Num_{1,i} m_{2,i}}$$

$$= n! \prod_{i=1}^{n} \frac{(i-1)!}{(Nu)^i}$$

where we have used (3.18).

We are now ready to derive the discrete Hirota Bilinear equation for Z_n. Writing

$$Z_n(x_1, x_2; u; N) = \frac{1}{\psi_n(u, N)} \int \Delta(m_1) \Delta(m_2)$$

$$(3.26)$$

$$\times \prod_{i=1}^{n} e^{-Num_{1,i} m_{2,i}} (1 - m_{1,i})^{-a_1} (1 - m_{2,i})^{-a_2} dm_{1,i} dm_{2,i}$$

with $a_k = Nx_k$, $k = 1, 2$, and using the basic definition of determinants

$$(3.27)$$
$$\prod_{i=1}^{n} (1 - m_{k,i})^{-a_k} \Delta(1 - m_k) = \det\left[(1 - m_{k,i})^{j-a_k-1}\right]_{1 \le i,j \le n}$$

$$= \sum_{\sigma \in S_n} \mathrm{sgn}(\sigma) \prod_{i=1}^{n} (1 - m_{k,i})^{\sigma(i)-a_k-1}$$

for $k = 1, 2$, and the shorthand notation

$$(3.28) \qquad Z_n(a_1, a_2) = Z_n(x_1, x_2; u; N) \qquad a_1 = Nx_1, a_2 = Nx_2$$

we finally get

$$Z_n(a_1, a_2) = \frac{1}{\psi_n(u, N)} \sum_{\sigma, \tau \in S_n} \mathrm{sgn}(\sigma\tau) \prod_{i=1}^{n} \int dm_{1,i} dm_{2,i}$$

$$(1 - m_{1,i})^{\sigma(i)-a_1-1} (1 - m_{2,i})^{\tau(i)-a_2-1} e^{-Num_{1,i} m_{2,i}}$$

$$(3.29) \qquad = \frac{n!}{\psi_n(u, N)} \sum_{\nu \in S_n} \mathrm{sgn}(\nu)$$

$$\prod_{i=1}^{n} \int dx dy (1 - x)^{i-a_1-1} (1 - y)^{\nu(i)-a_2-1} e^{-Nuxy}$$

where we have set $\nu = \tau\sigma^{-1}$, with the same signature as $\sigma\tau$, and explicitly factored out the sum over σ. Moreover, the dummy integration variables have been rebaptized x and y, and the integral can be computed by expanding the integrand as a power series of x, y and then using term by term the prescription (3.18). The partition function therefore takes the form

$$(3.30) \qquad Z_n(a_1, a_2) = \frac{n!}{\psi_n(u, N)} D_n(a_1, a_2)$$

where $D_n(a_1, a_2)$ is the $n \times n$ determinant

$$(3.31) \quad D_n(a_1, a_2) = \det\left[\int dx dy (1 - x)^{i-a_1-1} (1 - y)^{j-a_2-1} e^{-Nuxy}\right]_{1 \le i,j \le n}$$

and $\psi_n(u,N)/n! = D_n(0,0) = \prod_{1 \leq i \leq n}(i-1)!/(Nu)^i$.

The Hirota equation will be the consequence of the following general quadratic equation satisfied by the minors of the determinant D of any matrix of size $(n+1) \times (n+1)$. Denoting by $D_{i,j}$ the $n \times n$ minor of D obtained by erasing the i-th row and j-th column, and $D_{i_1,i_2;j_1,j_2}$ the $(n-1) \times (n-1)$ minor obtained by removing the rows i_1, i_2 and columns j_1, j_2, we have the quadratic relation

$$(3.32) \qquad D\,D_{1,n+1;1,n+1} \;=\; D_{n+1,n+1}\,D_{1,1} - D_{1,n+1}\,D_{n+1,1}.$$

This may be viewed as a particular case of the Plücker relations [20]. Applying (3.32) to $D = D_{n+1}(a_1+1, a_2+1)$, we immediately get

$$
\begin{aligned}
&D_{n+1}(a_1+1,a_2+1)D_{n-1}(a_1,a_2) \\
(3.33) \qquad &= D_n(a_1+1,a_2+1)D_n(a_1,a_2) - D_n(a_1,a_2+1)D_n(a_1+1,a_2)
\end{aligned}
$$

where we have used the explicit definition (3.31) to rewrite the various minors. Finally, using $\psi_{n+1}(u,N)\psi_{n-1}(u,N)/\psi_n(u,N)^2 = n/(Nu) = nt/N$, as a consequence of (3.25), (3.33) becomes (3.3) when expressed in terms of the $Z_n(a,a')$, and theorem 3 follows.

The equations (3.33) or (3.3) are known as discrete Hirota equations, playing a central role in integrable systems (see [20] for the general study of these and analogous equations). We obtain in this way an indirect relation between the foldable triangulations enumeration problem and integrable systems, a relation intriguingly reminiscent of that uncovered between lattice folding problems and integrable lattice models.

The Hirota equation (3.3) can be used to generate inductively the expansion (3.1) through (3.2). Indeed, writing

$$(3.34) \qquad\qquad\qquad f_n(a_1,a_2) \;=\; \mathrm{Log}\, Z_n(a_1,a_2)$$

and using the shorthand notation $\delta_x f(x) = f(x+1) - f(x)$, we can recast (3.3) into

$$(3.35) \qquad \delta_{a_1}\delta_{a_2} f_n(a_1,a_2) \;=\; -\,\mathrm{Log}\Big(1 - n\frac{t}{N}e^{\delta_n f_n(a_1+1,a_2+1)-\delta_n f_{n-1}(a_1,a_2)}\Big).$$

Now writing the formal t series expansion $f_n(a_1,a_2) = \sum_{m \geq 1}(t/N)^m \omega_{n,m}(a_1,a_2)$, (3.35) is nothing but a non-linear recursion relation for the coefficients $\omega_{n,m}(a_1,a_2)$, with the initial value $\omega_{n,1}(a_1,a_2) = na_1a_2$ (there is only one connected tri-colorable graph made of $A = 2$ triangles: those are glued along their edges, and the graph has one vertex of each color; this graph has genus zero, as indicated by $(t/N)na_1a_2 = N^2 tnx_1x_2$). It involves however a step of discrete integration wrt a_1 and a_2, but as we are dealing with polynomials of n, a_1, a_2, this step is readily done by noticing that all the $\omega_{n,m}(a_1,a_2)$ have at least a_1a_2 in factor, as there is always at least one edge connecting two vertices of color 1 and 2 in a given connected tri-colorable

graph. The first few ω's read

$$
\begin{aligned}
\omega_{n,1} &= na_1a_2 \\
\omega_{n,2} &= \frac{na_1a_2}{2}(n + a_1 + a_2) \\
\omega_{n,3} &= \frac{na_1a_2}{3}(n^2 + 3(a_1 + a_2)n + a_1^2 + 3a_1a_2 + a_2^2 + 1) \\
(3.36)\quad \omega_{n,4} &= \frac{na_1a_2}{4}(n^3 + 6(a_1 + a_2)n^2 + (6a_1^2 + 17a_1a_2 + 6a_2^2 + 5)n \\
&\quad + (a_1 + a_2)(a_1^2 + 5a_1a_2 + a_2^2 + 5)) \\
\omega_{n,5} &= \frac{na_1a_2}{5}(n^4 + 10(a_1 + a_2)n^3 + 5(4a_1^2 + 11a_1a_2 + 4a_2^2 + 3)n^2 \\
&\quad + 5(a_1 + a_2)(2a_1^2 + 9a_1a_2 + 2a_2^2 + 8)n \\
&\quad + a_1^4 + 10a_1^3a_2 + 20a_1^2a_2^2 + 10a_1a_2^3 + a_2^4 + 15a_1^2 + 40a_1a_2 + 15a_2^2 + 8).
\end{aligned}
$$

Note that our solution (3.36) displays the expected symmetry between $a_1 = Nx_1$, $a_2 = Nx_2$ and $n = Nx_3$, from the interpretation of $f_n(a_1, a_2) \equiv N^2 f(x_1, x_2, x_3; t; N)$ (3.1) as generating function for vertex-tricolored triangulations. This symmetry was however absolutely not manifest on (3.35). Note also that the genus expansion of f can be read off (3.36) by expressing the coefficients as

$$
\sum_{m \geq 1} (t/N)^m \omega_{n=Nx_3,m}(a_1 = Nx_1, a_2 = Nx_2) = \sum_{g \geq 0} N^{2-2g} f_g(x_1, x_2, x_3; t),
$$

where f_g denotes the genus g contribution to (3.1). For instance, we read from (3.36) the genus one contribution

$$
\begin{aligned}
f_1(x_1, x_2, x_3; t) &= \frac{t^3}{3}x_1x_2x_3 + \frac{5}{4}t^4x_1x_2x_3(x_1 + x_2 + x_3) \\
(3.37) &\quad + t^5x_1x_2x_3(3(x_1^2 + x_2^2 + x_3^2) + 8(x_1x_2 + x_2x_3 + x_1x_3)) + \ldots
\end{aligned}
$$

the first term corresponding to a triangulation of the torus with 6 triangles, sharing three vertices, and so on. We may also derive a partial differential equation for the genus zero part $f_0(x_1, x_2, x_3; t) = \lim_{N \to \infty} N^{-2} f(x_1, x_2, x_3; t; N)$ of (3.1) by substituting $\delta_{a_i} \to \partial_{x_i}/N$, $i = 1, 2$, and $\delta_n \to \partial_{x_3}/N$ into (3.35), which becomes:

$$
(3.38)\qquad \partial_{x_1}\partial_{x_2}f_0 = -\operatorname{Log}\left(1 - tx_3 e^{\partial_{x_3}(\partial_{x_1} + \partial_{x_2} + \partial_{x_3})f_0}\right).
$$

This allows for the computation of f_0 order by order in the t series expansion.

3.5. Direct Expansion and Genus Zero Result.
Let us start again from the expression (3.30) of the previous section, involving the determinant (3.31). Let us explicitly compute this determinant, by expanding

$$
(3.39)\qquad (1 - x)^{i-a-1} = \sum_{k \geq 0} \frac{\Gamma(k + a - i + 1)}{\Gamma(1 + a - i)} \frac{x^k}{k!}
$$

for $a = a_1, a_2$, and then using term-by-term the formal prescription (3.18), which results in

(3.40)

$$D_n(a_1, a_2) = \det\left[\sum_{k \geq 0} \frac{1}{k!} \frac{\Gamma(k + a_1 - i + 1)}{\Gamma(1 + a_1 - i)} \frac{\Gamma(k + a_2 - j + 1)}{\Gamma(1 + a_2 - j)}\left(\frac{t}{N}\right)^{k+1}\right]_{1 \leq i,j \leq n}$$

$$= \sum_{k_1,\ldots,k_n \geq 0} \prod_{i=1}^{n} \frac{(t/N)^{k_i+1}\Gamma(k_i + a_1 - i + 1)}{k_i!\,\Gamma(1 + a_1 - i)\Gamma(1 + a_2 - i)} \det\left[\Gamma(k_i + a_2 - j + 1)\right]_{1 \leq i,j \leq n}$$

where we have used the multilinearity of the determinant to extract line by line the summations over k's. Factoring $\Gamma(k_i + a_2 - n + 1)$ out of each line (number i) of the remaining determinant, we are left with a determinant of the form

(3.41) $\det\left[(k_i + a_2 - j)(k_i + a_2 - j - 1)...(k_i + a_2 - n + 1)\right] = \det\left[q_{n-j}(k_i)\right]$

where the polynomials $q_m(x) = x^m$+lower degree are monic. Using multilinearity and the fact that the determinant is alternate, we may easily derive that $\det[q_{n-j}(k_i)] = \det[k_i^{j-1}]$, which is nothing but the Vandermonde determinant of the k_i's, namely $\Delta(k) \equiv \Delta(k_1, k_2, ..., k_n)$. We finally get the expansion of the determinant (3.31)

(3.42) $$D_n(a_1, a_2) = \sum_{k_1,\ldots,k_n \geq 0} \prod_{i=1}^{n} \frac{t^{k_i+1}\Gamma(k_i + a_1 - i + 1)\Gamma(k_i + a_2 - n + 1)}{N^{k_i+1}k_i!\,\Gamma(1 + a_1 - i)\Gamma(1 + a_2 - i)}\Delta(k).$$

Using the skew-symmetry of $\Delta(k)$, we can also write

(3.43) $$D_n(a_1, a_2) = \frac{1}{n!} \sum_{k_1,\ldots,k_n \geq 0} \prod_{i=1}^{n} \frac{1}{k_i!} \frac{(t/N)^{k_i+1}}{\Gamma(1 + a_1 - i)} \frac{\Gamma(k_i + a_2 - n + 1)}{\Gamma(1 + a_2 - i)}$$

$$\times \Delta(k) \det[\Gamma(k_i + a_1 - j + 1)]_{1 \leq i,j \leq n}.$$

Factoring again $\Gamma(k_i + a_1 - n + 1)$ off each line (number i) of the last determinant, and repeating the above trick, we finally get

(3.44) $$D_n(a_1, a_2) = \frac{1}{n!} \sum_{k_1,\ldots,k_n \geq 0} \Delta(k)^2 \prod_{i=1}^{n}(t/N)^{k_i+1}\frac{1}{k_i!} \prod_{r=1}^{2} \frac{\Gamma(k_i + a_r - n + 1)}{\Gamma(1 + a_r - i)}$$

or, using (3.30),

(3.45) $$Z_n(a_1, a_2) = \sum_{k_1,\ldots,k_n \geq 0} \Delta(k)^2 \prod_{i=1}^{n} \frac{(t/N)^{k_i+1-i}}{i!\,k_i!} \prod_{r=1}^{2} \frac{\Gamma(k_i + a_r - n + 1)}{\Gamma(1 + a_r - i)}.$$

The expansion (3.45) yields the desired genus expansion (3.1) upon the substitution $a_i = Nx_i$, $i = 1, 2$ and $n = Nx_3$ in the result, once expressed as a polynomial of n, a_1, a_2. For more efficiency, the sum (3.45) may be reduced to one over strictly increasing sequences $0 \leq k_1 < k_2 < k_3 < ... < k_n$, and yields many interesting results [18], including a new proof of some earlier result [23], corresponding to the case $x_1 = x_2 = x_3$. One of them is the large N, genus zero expansion of $f_0(x_1, x_2, x_3; t)$, solution of (3.38). The large N asymptotics of (3.45) in the saddle-point approximation show that $Z_n(a_1, a_2) \sim e^{N^2 f_0}$, and finally lead to the result (3.5) (see [18] for a detailed proof of theorem 4).

Theorem 4 gives access to the study of the singularities of f_0 as a series of t, in terms of the parameters x_i. In particular, it is easy to show that the series

displays generically a finite convergence radius, an ordinary feature of quantum gravity. A last remark is in order: from eqn.(3.5), it appears that $F_i(x_1, x_2, x_3; t)$ is the generating function for vertex-tricolored rooted trees with a root of color i (such that any two vertices connected with an edge have distinct colors). Our result links this rather simple function to the generating function of genus zero tricolored triangulations.

3.6. Folding Foldable Triangulations. Another interesting matrix model serves as generating function for the edge-tricolored triangulations. It reads

$$(3.46) \qquad Z_{\text{edge}} = \int dM_1 dM_2 dM_3 e^{-N \operatorname{Tr}(\sum_{i=1}^3 \frac{M_i^2}{2} - z(M_1 M_2 M_3 + M_1 M_3 M_2))}$$

where the integral extends over $N \times N$ Hermitian matrices. As before, we may expand (3.46) as a formal power series of z, and compute the coefficient of z^n as a triple Gaussian integral, by use of the Feynmann diagrams and rules easily read off (3.46). As only "diagonal" propagators $\langle M_i M_j \rangle \propto \delta_{ij}$ are allowed, the graphs have cubic vertices only, and edges painted with colors $1, 2, 3$ according to the corresponding matrix index. Dually, these are nothing but edge-tricolored triangulations, such that the three edges of each triangular face have distinct colors. This model is the quantum-gravitational version of the edge-tricoloring problem solved by Baxter [12] with entropy (2.10), and was solved iteratively in [19].

It is however *not* the quantum-gravitational version of our triangular lattice folding problem. Indeed, (3.46) does not extend over *foldable* triangulations, but over *all* triangulations. A correct model for the study of folding of fluid triangulations should include both the foldability constraint and the edge-tricoloring. The problem of finding a good matrix formulation of such a model is still open. As a first hint, let us write a matrix model valid only as far as genus zero results are concerned. We have seen that the foldability constraint in genus zero boils down to the fact that the triangulations have only vertices of even valency. The suitable modification of (3.46) to include this constraint goes as follows. Let us restrict ourselves to matrices of even size $N = 2P$. Let $\Lambda = \operatorname{diag}(\lambda_1, \lambda_2, ..., \lambda_N)$ be a real diagonal matrix such that $\theta_{2k+1} = \operatorname{Tr}(\Lambda^{-2k-1})/N = 0$ and $\theta_{2k} = \operatorname{Tr}(\Lambda^{-2k})/N$ are a collection of non-vanishing real parameters (for instance, we can take $\lambda_{2i} = -\lambda_{2i-1} = 1$ for $i = 1, 2, ..., P$, in which case $\theta_{2k} = 1$ for all k). The modified matrix model now reads

$$(3.47) \qquad Z_{\text{fold}} = \int dM_1 dM_2 dM_3 e^{-N \operatorname{Tr}(\sum_{i=1}^3 \frac{(\Lambda M_i)^2}{2} - z(M_1 M_2 M_3 + M_1 M_3 M_2))}.$$

Repeating the calculation of (3.47) as a formal series expansion of z, we still have to sum over graphs with only trivalent vertices and connected with edges colored $1, 2, 3$ corresponding to the propagators

$$(3.48) \qquad \langle (M_a)_{ij} (M_b)_{kl} \rangle = \frac{1}{N \lambda_i \lambda_j} \delta_{ab} \delta_{il} \delta_{jk}.$$

Indeed, the diagonal quadratic form Q: $\frac{N}{2} \operatorname{Tr}(\Lambda M)^2 = \frac{1}{2} \sum Q_{ij;lk} M_{ij} M_{kl}$ has a diagonal inverse with elements $1/(N \lambda_i \lambda_j)$. Note that the factor $1/\lambda_i$ in (3.48) can be thought of as an extra decoration of the oriented line carrying the index i. When we collect all the factors of N and sum over all indices running over the oriented loops around each face of the graph, we get a total of N^{v-e}, v the total number of vertices, e that of edges of the graph, but from each loop of length ℓ (i.e. made of ℓ edges) we now get a factor $\sum_{i=1}^N \lambda_i^{-\ell}$. We also get a factor z per vertex. In the

dual picture, we therefore sum over triangulations with tricolored edges and whose ℓ-valent vertices receive a weight $\mathrm{Tr}(\Lambda^{-\ell})$. With the above restrictions on Λ, we see that only even vertices are allowed and that they receive a weight $N\theta_\ell$. We finally get

$$(3.49) \qquad Z_{\text{ fold}} \ = \ \sum_{\substack{\text{edge-tricolored}\\ \text{even triangulations } T}} \frac{1}{|\ \mathrm{Aut}(T)|} N^{2-2g(T)} z^{A(T)} \prod_{\text{vertices}} \theta_\ell$$

where the sum extends over triangulations with even vertices, and each vertex is weighed by θ_ℓ, ℓ its valency. The computation of (3.47) is still an open problem.

More generally, using the colored cluster formulation of the various two- and higher-dimensional problems that we have addressed, we may always write their quantum-gravitational version as some multi-matrix models (typically, the increase in dimension will just result in more matrices and more allowed vertices). The foldability constraint however will always have to be implemented "by hand". For instance, in the case of the two-dimensional square-diagonal folding, we may introduce the quantum-gravitational version of the colored cluster model of Fig.5, in the form of a matrix integral

$$Z_{\text{ cluster}} \ = \ \int dM_1 dM_2 dP_1 dP_2 e^{-N\ \mathrm{Tr}\ V(M_1,M_2,P_1,P_2)}$$

$$(3.50) \qquad V(M_1,M_2,P_1,P_2) \ = \ \frac{1}{2} \sum_{i=1}^{2} M_i^2 + P_i^2 - t(M_i^4 + P_i^4)$$

$$- \frac{1}{2} \sum_{i,j=1}^{2} t(M_i^2 P_j^2 + M_i P_j M_i P_j)$$

where the quartic terms represent the vertices of the last line of Fig.5, M matrices stand for clusters of color 1, P matrices for color 2, and within each color the matrices M_1, M_2 stand for the signs ± 1. This is not sufficient however to formulate the fluid square-diagonal folding problem. Indeed, we are now considering graphs made of tessellations with square faces (of long edges), each containing 4 short edges. As before, foldability implies that there always be an even number of long edges adjacent to each vertex, hence that in the dual picture each face have an even valency. We need therefore to modify the propagators in (3.50) in a way analogous to (3.47), namely $M_i^2 \to (\Lambda M_i)^2$ and $P_i^2 \to (\Lambda P_i)^2$, with the same Λ as before.

4. Polymer folding: Meanders

We now address the folding problem of polymer chains. Such a chain is ideally described by a chain of identical line segments attached by their ends, which serve as hinges between adjacent segments. Think of a single strip of stamps, which can be folded along the edges common to each neighboring stamp. We will distinguish between closed and open polymers according to whether the chain forms a loop or is open with two free ends. We will be addressing the *compact self-avoiding* folding of such objects, namely studying the various ways in which the polymer can be completely folded onto one of its segments. Note that a closed compactly foldable polymer must have an even number of segments.
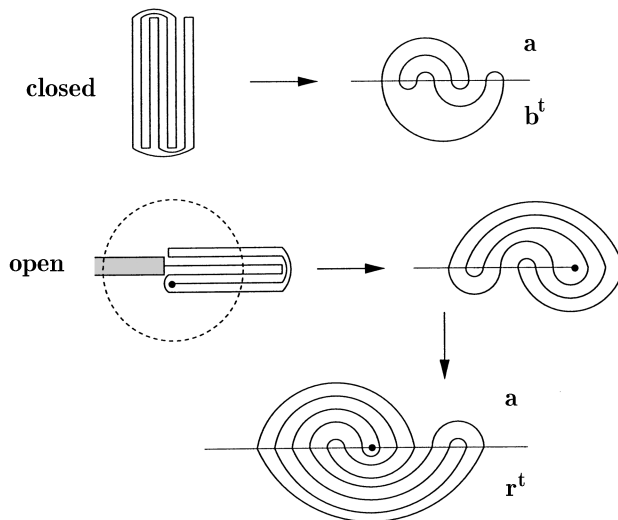
FIGURE 13. Two compactly folded polymers and the corresponding meanders. The first example is a closed polymer with 8 segments, and corresponds to a meander of order 8, viewed as the superposition of two arch configurations of order 8, a and the reflection b^t of b wrt the river. The second example is an open polymer with 6 segments, and corresponds to a semi-meander of order 7, itself viewed as a particular meander of order 14 after opening the river. The latter is the superposition of two arch configurations of order 14, a and the reflection r^t of the rainbow diagram wrt the river. The winding is 3 and corresponds to the number of arches passing above the source of the river.

4.1. Definitions. To distinguish between the various ways of compactly folding a closed polymer, we will represent the folded object as a *meander of order* $2n$, namely a planar configuration of a non-self-intersecting loop (road) intersecting a line (river) through a given number $2n$ of distinct points on the line (bridges). All the intersections are simple, and the meanders are considered up to smooth deformations preserving their topology. The total number of meanders of order $2n$ is denoted by M_n. This number is known to behave for large n as [29] [33]

$$(4.1) \qquad\qquad M_n \sim C \frac{R^{2n}}{n^\alpha}.$$

One of the most remarkable predictions to this day is the exact value of the meander configuration exponent [36]

$$(4.2) \qquad\qquad \alpha = \frac{29 + \sqrt{145}}{12}.$$

To visualize the relation between compactly folded closed polymers and meanders, it is simplest to imagine drawing a line perpendicular to the segments forming the folded polymer with a total of $2n$ intersections (each segment intersects the line once), and then separating the various segments (see Fig.13).

In the case of an open polymer with say $n-1$ segments, let us attach one of its ends to a wall or a support (see Fig.13), so as to prevent the polymer from winding around that end (this is exactly the situation in a strip of stamps, attached by one end to its support). Starting from a compactly folded configuration, let us draw this time a circle that intersects each of the n segments once, and also intersects the support once. Extending the polymer so as to let it form a half-line with origin its free end, we form a planar configuration of a non-self-intersecting loop (road) crossing a half-line (river with a source) through n points. These configurations considered up to smooth deformations preserving the topology are called *semi-meanders of order n* (see Fig.13 for an illustration). The total number of semi-meanders of order n is denoted by $\bar{M}_n$. Similarly to (4.1), we have large n asymptotics

$$(4.3) \qquad \bar{M}_n \sim \bar{C} \frac{\bar{R}^n}{n^{\bar{\alpha}}}$$

where it is expected that $\bar{R} = R$ [33] and the semi-meander configuration exponent is predicted to read [36]

$$(4.4) \qquad \bar{\alpha} = 1 + \frac{1}{24}\sqrt{11}(\sqrt{5} + \sqrt{29}).$$

We may also define the winding of a semi-meander as the minimum number of intersections one has to make when connecting the source of the river to infinity.

A unifying way of considering meanders is to view them as the superposition of their upper and lower halves, delimited by the river. In a meander of order $2n$, the upper half say is made of n non-intersecting arches connecting bridges by pairs. Such a configuration is called an arch configuration of order $2n$. The set of arch configurations of order $2n$ is denoted by A_{2n}. It is straightforward to show that $|A_{2n}| = c_n = (2n)!/(n!(n+1)!)$, the n-th Catalan number. The lower half of the meander is also an arch configuration of order $2n$, but upside-down, i.e. reflected wrt the river. The semi-meanders of order n can be viewed as particular meanders of order $2n$ by simply opening up the half-line into a line (see Fig.13 for an example), and by using the semi-meander loop to form the connections in the upper-half plane between the (now doubled) bridges, whereas the lower-half is just made of the reflected "rainbow" arch configuration which connects the bridges i and $2n+1-i$. In that formulation, the winding of the semi-meander is simply the number of arches passing above the former source, now the middle of the river.

This formulation leads to an immediate generalization to multi-component meanders (resp. semi-meanders), obtained by superposing any pairs of arch configurations (a, b^t) (resp. any arch configuration a with r^t). The resulting multi-component meander (resp. semi-meander) has a number $c(a, b)$ (resp. $c(a) \equiv c(a, r)$) of connected components of road. This leads to the introduction of the meander and semi-meander partition functions of a given order

$$
\begin{aligned}
m_{2n}(q) &= \sum_{a,b \in A_{2n}} q^{c(a,b)} \\
(4.5) \qquad \bar{m}_n(q) &= \sum_{a \in A_{2n}} q^{c(a)}
\end{aligned}
$$

also referred to as meander and semi-meander polynomials. As a direct consequence of the definition, we have $m_{2n}(1) = (c_n)^2 \sim 4^{2n}/(\pi n^3)$ and $\bar{m}_n(1) =$
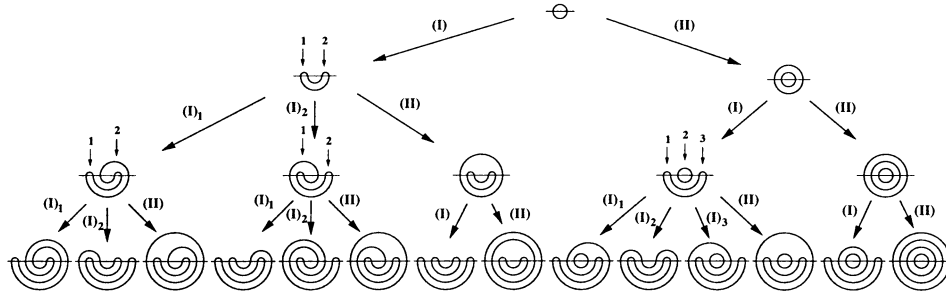
FIGURE 14. The tree of semi-meanders, down to order 4. We have represented the only semi-meander of order 2 as the root. Each branch corresponds to an operation (I) or (II). We have indicated the exterior arches giving rise to the various moves (I). The number of connected components of a leaf is one plus the number of (II) moves from the root.

$c_n \sim 4^n/(\sqrt{\pi}n^{3/2})$, where the large n asymptotics are obtained by use of Stirling's formula. Note that multi-component meanders or semi-meanders correspond to compact folding configurations of several possibly interlocked polymers, and the partition functions (4.5) include a weight q per polymer.

One way of computing the polynomials (4.5) numerically uses an induction process within the framework of semi-meanders. Indeed, meanders can be seen as particular cases of semi-meanders with no winding, so it is sufficient to develop some induction for semi-meanders. The inductive step will produce all semi-meanders of order $n+1$ from those of order n, and keep track of their numbers of connected components, winding, and any property we want to analyze statistically. It goes as follows. We start from a semi-meander S_n of order n, say the superposition of some $a_n \in A_{2n}$ and of the rainbow of order $2n$, r_n. We may now produce semi-meanders of order $n+1$ by adding two bridges along the river (a bridge labelled 0 on the left, and one labelled $2n+1$ on the right), connected from below by an arch (thus forming the rainbow r_{n+1} of order $2n+2$ in its lower half), in either of the two following ways:

(I) Pick any exterior arch of S_n, i.e. an arch with no other arch passing above it, say connecting bridges labelled i and j, $i < j$, and replace it by two arches connecting respectively the bridges 0 to i and j and $2n+1$. This operation preserves the number of connected components of road.

(II) Connect the bridges 0 and $2n+1$ in the upper-half plane: this adds one connected component of road (a circle around S_n).

It is easily checked that (I) and (II) above produce exactly all the semi-meanders of order $n+1$ from those of order n. Note that a given semi-meander of order $2n$ gives rise to $e+1$ meanders of order $2n+2$, if e denotes its total number of exterior arches (those adjacent to the infinite face delimited by the upper-half plane and the semi-meander). We have represented in Fig.14 the tree of semi-meanders, with the unique semi-meander of order 2 at its root, and we have indicated the branches corresponding to the operations (I) and (II) above.

The moves (I) and (II) are easily implemented on a computer. If we look only for connected semi-meanders, we only have to consider (I), and a typical (Fortran) program of enumeration would look as follows.

```
      PARAMETER(nmax = 14)                  ! maximal order
      INTEGER A(-nmax + 1 : nmax)           ! arch representation
      INTEGER Sm(nmax)                      ! semi-meander counter
      INTEGER n                             ! current depth (or order)
      INTEGER j                             ! next branch to visit
      DATA n, Sm /0, nmax*0/                ! n and Sm initialized to 0
      A(0) = 1                              ! root
      A(1) = 0
    2 n = n + 1                             ! a new node is visited
      Sm(n) = Sm(n) + 1
      j = -n + 1                            ! leftmost (exterior) arch
    1 IF((n.EQ.nmax).OR.(j.EQ.n+1)) GOTO 3  ! up or down ?
      A(A(j)) = n+1                         ! go down with move (I)
      A(n+1) = A(j)
      A(j) = -n
      A(-n) = j
      GOTO 2
    3 A(A(-n+1)) = A(n)                      ! going up
      A(A(n)) = A(-n+1)
      j = A(n)+1                            ! next arch to break
      n = n - 1
      IF (n .GT. 1) GOTO 1
      PRINT '(i3, i15)', (n, Sm(n), n = 1, nmax)
      END
```

Note that we have coded the upper arch configuration of order $2n$ by labelling its bridges from $-n+1$ to n, and by a map $j \to A(j)$ expressing the other bridge $A(j)$ connected to the bridge j by an arch. The output is the list of numbers $Sm(n)$ of connected semi-meanders of order n. The program above manages to visit all the leaves of the tree of connected semi-meanders. The best estimates of the meandric numbers using this method can be found in [33] and [34].

Another more powerful method of enumeration was introduced recently in [35], which is closer in spirit to the methods of integrable lattice models. It is based on the introduction of a transfer matrix for meanders as follows. Take any meander with say $2n$ bridges (see Fig.15 (a), with $n = 6$). Then cut the meander into vertical "time-slices", each containing exactly one bridge, as shown in Fig.15 (a). We may now construct the set of all meanders by concatenating all possible slices. More precisely, we represent a portion of meander say to the left of the pth slice by encoding all the connections of points along the vertical line between the slices $p-1$ and p to the left that we may represent by arches connecting points by pairs, as shown in Fig.15 (b) for the 13 successive "states" into which the meander is decomposed. When we add the pth slice, this configuration may evolve according to any of the four possibilities depicted in Fig.15 (c). We therefore have a simple matrix connecting various "states", i.e. configurations of points paired along a vertical line, through arches drawn on their left. Note that the position of the river must also be specified on such states. This leads to a natural method of
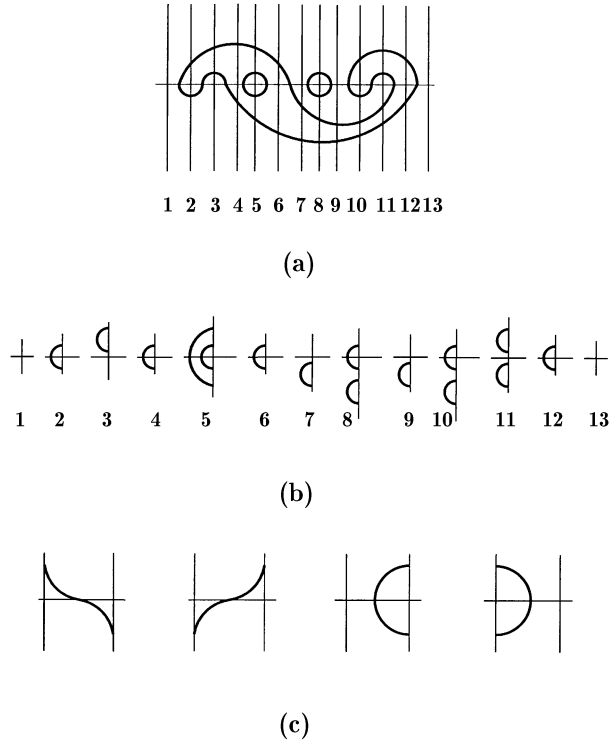
(a)

(b)

(c)

FIGURE 15. The transfer matrix for meanders. We have represented in (a) a typical meander together with its vertical slice decomposition. The successive corresponding states are listed in (b). The mechanism of the transfer matrix is as follows: it acts on the states of (b) in the four possible ways of (c), according to the structure of the added slice, entirely determined by its local configuration close to the river. Counting meanders is realized by iterating this transfer matrix $2n$ times. In the example of (b), we must start from the vacuum state 1 and end up with the same state 13, after concatenating 12 intermediate slices.

enumeration of meanders that is much more efficient than that of hopping on the tree of semi-meanders. One drawback is that although it is better adapted to the enumeration of meanders, it is not as efficient with semi-meanders [39]. The best numerical data to this date are the one-component meander numbers for up to $48 = 2 \times 24$ bridges [35], multi-component meanders up to $40 = 2 \times 20$ bridges and multi-component semi-meanders up to 33 bridges [39].

Such numerical results give access to good approximations to the large order asymptotics of the meander and semi-meander polynomial (4.5), namely

$$(4.6) \qquad m_{2n}(q) \ \sim \ C(q) \frac{R(q)^{2n}}{n^{\alpha(q)}}$$
$$\bar{m}_n(q) \ \sim \ \bar{C}(q) \frac{\bar{R}(q)^n}{n^{\bar{\alpha}(q)}}$$

with some thermodynamic partition functions per bridge $R(q)$ and $\bar{R}(q)$ and some configuration exponents $\alpha(q)$ and $\bar{\alpha}(q)$. Comparing with the above-mentioned values at $q = 1$, we get

$$(4.7) \qquad\qquad R(1) = \bar{R}(1) = 4 \qquad \alpha(1) = 3 \quad \bar{\alpha}(1) = 3/2.$$

Actually a detailed study of the large q behavior of (4.5), namely the case of a large number of connected components has led to the explicit form of the few largest order terms in (4.5), themselves leading to an explicit large q series expansion for $R(q)$ and $\bar{R}(q)$, reading [33]

$$
\begin{aligned}
R(q) \;=\;& 2\sqrt{q}\Big(1 + \frac{1}{q} + \frac{3}{2q^2} - \frac{3}{2q^3} - \frac{29}{8q^4} - \frac{81}{8q^5} - \frac{89}{16q^6} + O(\tfrac{1}{q^7})\Big) \\
(4.8)\qquad \bar{R}(q) \;=\;& q + 1 + \frac{2}{q} + \frac{2}{q^2} + \frac{2}{q^3} - \frac{4}{q^5} - \frac{8}{q^6} - \frac{12}{q^7} - \frac{10}{q^8} - \frac{4}{q^9} + \frac{12}{q^{10}} + \frac{46}{q^{11}} \\
& + \frac{98}{q^{12}} + \frac{154}{q^{13}} + \frac{124}{q^{14}} + \frac{10}{q^{15}} - \frac{102}{q^{16}} + \frac{20}{q^{17}} - \frac{64}{q^{18}} + O(\tfrac{1}{q^{19}}).
\end{aligned}
$$

This shows a very different behavior between meanders and semi-meanders for large q: the reason for that is the relevance of winding, namely the predominance within semi-meanders with large numbers of components of configurations with large winding numbers (typically proportional to n). As the winding is forced to take the value 0 in meanders, this explains the very different behaviors of $R(q)$ and $\bar{R}(q)$.

It has been noted in [33] however that this is true only for q larger than a critical value q_c, (computed to be $q_c = 2\cos\big(\pi(\sqrt{97} - 1)/48\big)$ in [36] [37]). In the region $0 \leq q \leq q_c$ the winding becomes irrelevant, and we have $R(q) = \bar{R}(q)$ (see (4.7) for $q = 1$). This change of behavior has been identified in [33] as a physical continuous phase transition. So we expect the large q expansions (4.8) to break down at $q = q_c^+$, which is actually observed on their plots.

4.2. Various Representations. To go beyond numerical work, we will first have to find a good mathematical representation for meanders and semi-meanders. In this section we present three very different formulations of the polynomials (4.5): the first one is purely combinatorial, within the framework of the symmetric group $\mathbf{S}_n$; the second is inspired by matrix model techniques such as those exposed in Sect.3; the third one combines the idea already obvious from the matrix model formulation that meanders may be viewed as random graphs or dually as tessellated random surfaces, expressing the coupling of a certain two-dimensional lattice model to quantum gravity. The latter approach allows for precise estimates of meander configuration exponents in the limit of large numbers of bridges.

Symmetric group expression: The arch configurations of order $2n$ may be represented, by numbering the bridges $1, 2, ..., 2n$, as permutations of S_{2n}, with only cycles of length 2, namely elements of the class $[2^n]$ (see Fig.16 for an example). Indeed, each such cycle (ij) represents the pairing between bridges i and j. But not all such permutations are "planar", i.e. represented pictorially by arch configurations of order $2n$. Let us introduce the "shift" permutation $\tau(i) = i + 1$ for $i = 1, 2, ..., 2n - 1$ and $\tau(2n) = 1$. Then the planarity condition for a given $\sigma \in S_{2n}$ translates into the fact that the arch configuration forms a tessellation of the upper-half plane, with n arches and $n + 1$ faces, as illustrated in Fig.16 for $n = 3$. Each such face is easily seen to correspond to a cycle of the permutation $\tau\sigma$. Hence the
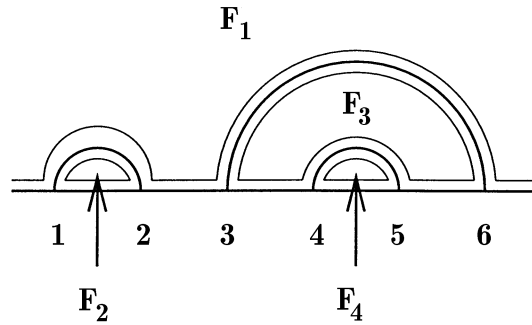
FIGURE 16. A sample arch configuration of order 6 defines a tessellation of the upper half plane with 4 faces. The corresponding permutation of S_6 reads $\sigma = (12)(36)(45) \in [2^3]$. Each face of the tessellation corresponds to a cycle of the permutation $\tau\sigma = (13)(2)(46)(5)$, with the correspondence $F_1 \to (13)$, $F_2 \to (2)$, $F_3 \to (46)$ and $F_4 \to (5)$.

planarity condition is simply that $\tau\sigma$ have exactly $n + 1$ cycles. So we may view the arch configurations of order $2n$ as the set

$$(4.9) \qquad T_{2n} = \{\sigma \in [2^n] | \tau\sigma \in [i^{\mu_i}], \sum \mu_i = n + 1\}.$$

Given a pair of such permutations (σ, σ'), the resulting meander's road components are described by simply composing the two permutations σ and σ'. A connected component of road is easily seen to correspond to some cycle of the permutation $\sigma\sigma'$. Hence enumerating those cycles amounts to counting the connected components. Note that each component corresponds to two cycles of equal length, one with bridges of even labels and one with bridges of odd labels.

In particular, connected meanders correspond to $\sigma, \sigma' \in T_{2n}$, such that $\sigma\sigma' \in [n^2]$; namely the permutation $\sigma\sigma'$ has two cycles of equal length n, both corresponding to the same unique road.

Matrix model for meanders: In the same spirit as in Sect.3, let us construct a Hermitian matrix integral that generates the meander polynomials. The computation of such an integral must involve fatgraphs with double-line edges, which we will eventually interpret as the river(s) and the road(s). Let us paint in white the "river" edges, and in black the "road" edges. We therefore have a "black and white" graph made of black and white loops which intersect each other through simple intersections. To assign a weight say b per black loop (component of road) and w per white loop (component of river), the simplest way is to use a "replica" trick: introduce b "black" Hermitian matrices $B_1, B_2, ..., B_b$ and w "white" Hermitian matrices $W_1, W_2, ..., W_w$, all of size $N \times N$, with the only non-vanishing propagators (allowed edges)

$$(4.10) \qquad\qquad \text{white edges}: \quad \langle W_i W_j \rangle = \frac{1}{N}\delta_{i,j}$$

$$\text{black edges}: \quad \langle B_i B_j \rangle = \frac{1}{N}\delta_{i,j}$$

and only simple intersection vertices $\text{Tr}(W_i B_j W_i B_j)$. The case of a unique river will be recovered by taking the limit $w \to 0$. This suggests introducing the "black and white" matrix integral

$$(4.11) \qquad Z_{b,w}(N;x) \;=\; \int \prod_{i=1}^{b} dB_i \prod_{j=1}^{w} dW_j \, e^{-N \, \text{Tr} \, V(\{B_i\},\{W_j\})}$$

$$V(\{B_i\},\{W_j\}) \;=\; \frac{1}{2}\Big(\sum_{i=1}^{b} B_i^2 + \sum_{j=1}^{w} W_j^2 - x \sum_{i=1}^{b} \sum_{j=1}^{w} B_i W_j B_i W_j \Big).$$

The corresponding free energy may be formally expanded as a sum over all possible connected black and white graphs as

$$(4.12) \qquad F_{b,w}(N;x) \;=\; \frac{1}{N^2} \, \text{Log} \, Z_{b,w}(N;x)$$

$$= \sum_{\text{black \& white } \Gamma} \frac{1}{|\,\text{Aut}(\Gamma)|} N^{-2g(\Gamma)} x^{v(\Gamma)} b^{L_b(\Gamma)} w^{L_w(\Gamma)}$$

where, as in Sect.3, $g(\Gamma), v(\Gamma)$ and $\text{Aut}(\Gamma)$ denote respectively the genus, number of vertices, and symmetry group of Γ, whereas $L_b(\Gamma)$ and $L_w(\Gamma)$ denote respectively the numbers of black and white loops of resp. black and white edges in Γ. To get a generating function for meander polynomials from (4.12), we simply have to take $N \to \infty$ to retain only the planar graphs (genus zero), and then compute only the coefficient of w in the resulting expression as a power series of w, which leads to

$$(4.13) \qquad \lim_{N \to \infty} \frac{\partial F_{b,w}(N;x)}{\partial w}\bigg|_{w=0} \;=\; \sum_{n=1}^{\infty} \frac{x^{2n}}{4n} \, m_{2n}(b)$$

where we simply have identified the symmetry group of the resulting meanders to be $\mathbb{Z}_{2n} \times \mathbb{Z}_2$ for the cyclic symmetry (the river forms a loop), and the symmetry between inside and outside of that loop. Note also that keeping N finite, we get an all genus expansion

$$(4.14) \qquad \frac{\partial F_{b,w}(N;x)}{\partial w}\bigg|_{w=0} \;=\; \sum_{g \geq 0} N^{-2g} \sum_{n=1}^{\infty} \frac{x^n}{2n} \, m_n^{(g)}(b)$$

where we have defined the genus g meander polynomials $m_n^{(g)}(b)$. This leads to a natural higher genus generalization of meanders.

More generally, we may keep b and w finite and consider the generating function

$$(4.15) \qquad F_{b,w}(x) = \lim_{N \to \infty} F_{b,w}(N;x) = \sum_{n \geq 1} \frac{x^{2n}}{4n} m_{2n}(b,w)$$

of the multi-river and multicomponent meander polynomials $m_{2n}(b,w)$.

Unfortunately, the integral (4.11) has not been calculated directly yet. The best estimates known to this day [30] involve doing first the integration over say the W's, which is simply Gaussian, and then expanding the result as a sum over traces of products of black matrices, integrated wrt a Gaussian integration measure. This in turn can be evaluated by use of recursion relations, which have the same flavor as our initial recursion relations for meanders (see [30] for details).

Meanders as a gravitational Fully-Packed loop model:

In a recent work [36] it has been noticed that the B&W matrix model (4.11) is the natural random surface (i.e. gravitational) version of some Fully Packed
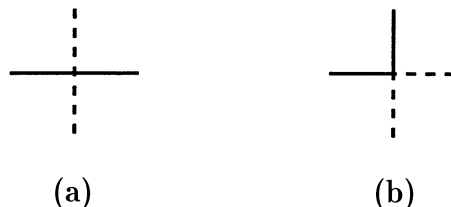
(a)   **(b)**

FIGURE 17. The two vertices of the FPL model, up to rotations:
(a) "crossing" and (b) "avoiding".

loop model on the square lattice. The latter is defined by assigning a color (B or W) to each edge of the square lattice in such a way that two edges of each color meet at each vertex. These edges then form (Fully Packed) loops, each of which is assigned a weight w or b for white and black loops respectively. The model is called the $\mathrm{FPL}^2(b, w)$ model [38]. When defined on a random surface of genus zero, the FPL model assigns colors to the edges of a random fatgraph with only vertices of the form $BWBW$ (crossing) or $BBWW$ (avoiding) depicted in Fig.17 (a) and (b) respectively. The B&W model (4.11) does not have the second kind of vertices. Therefore the original Fully Packed loop model must be further restricted.

The detailed study of the $\mathrm{FPL}^2(b, w)$ model shows two remarkable facts: (i) it is critical for all values of $0 \leq b, w \leq 2$, and (ii) it is represented in the continuum limit by a conformal field theory with central charge

$$(4.16) \qquad c_{FPL}(b, w) = 3 - 6\left(\frac{e^2}{1 - e} + \frac{f^2}{1 - f}\right)$$

where $w = 2\cos \pi e$ and $b = 2 \cos \pi f$. This was proved by mapping the $\mathrm{FPL}^2(p, q)$ model onto a three-dimensional height model, where the heights are defined in the center of each face of the square lattice, with an Ampère-like rule prescribing the transitions from one face to its neighbors, according to the configuration of the edge crossed. In the continuum limit, the height variable becomes a three-dimensional free field (conformal field theory with central charge $c = 3$), and the corrective weights assigning the factors b and w per loop of each color account for the correction (4.16) of c by "electric" charges e, f. The fact that this height variable is three-dimensional relies crucially on the vertex-bicolorability of the square lattice, which allows us to define the above-mentioned Ampère-like rules unequivocally. To describe the gravitational version of the FPL model, we must replace the square lattice by an arbitrary four-valent graph that is generically no longer vertex-bicolorable. This further restricts the height variable to live in two dimensions rather than three, and makes the "avoiding" vertex of Fig.17 (b) irrelevant, as say the heights in its SW and NE corners are equal; therefore, the two opposite faces may as well communicate with each other so as to form only one, and the vertex may consequently be undone. The correct formula for the central charge of the flat space non-bicolorable Fully Packed Loop theory is therefore

$$c(b, w) = 2 - 6\left(\frac{e^2}{1 - e} + \frac{f^2}{1 - f}\right)$$

$$(4.17) \qquad w = 2 \cos \pi e$$

$$b = 2 \cos \pi f$$

with $e, f \in [0, 1/2]$ (i.e. $0 \leq b, w \leq 2$), simply one less than c_{FPL} (4.16). We therefore state that the B&W model is described in the planar (large N) limit by the gravitational version of a conformal theory with central charge (4.17), namely the same theory defined on fluctuating surfaces that have to be summed over statistically. Note that the central charge (4.17) is identical to that of the Fully-Packed model of Sect. 2.6, with $\beta_1 = b$, $\beta_2 = w$. This latter model is easily seen to be also a restriction of the $FPL^2(b, w)$ model, in which the height variable is forced to live in two dimensions too. Therefore, in a sense, we are now dealing with the gravitational version of the square-diagonal lattice phantom folding as well.

The coupling to gravity of a conformal theory with central charge $c \leq 1$ has been extensively studied within the context of non-critical string theory (see the review [17] for instance). The gravitational theory has a new parameter x, called the cosmological constant, coupled to the area of the surfaces we have to sum over. More precisely, the free energy for a conformal theory coupled to gravity in genus zero reads

$$(4.18) \qquad F = \operatorname{Log} Z = \sum_{A \geq 0} x^A \sum_{\substack{\text{connected surfaces } \Gamma \\ \text{of area } A}} Z_{CFT}(\Gamma)$$

where $Z_{CFT}(\Gamma)$ denotes the partition function of the conformal theory on the genus zero connected surface Γ. Comparing Z with the B&W model partition function (4.11), we see that x plays the role of cosmological constant, as $n = A$ are the areas of the tessellations dual to the fatgraphs of the model. When the conformal theory has central charge c, the free energy (4.18) has been shown to have a singularity of the form [40]:

$$(4.19) \qquad F \sim (x_c - x)^{2-\gamma} \qquad \gamma = \frac{1}{12}(c - 1 - \sqrt{(1-c)(25-c)})$$

when x approaches some critical value x_c. This is easily translated into the large area asymptotics of the partition function of the model on surfaces of fixed area

$$(4.20) \qquad F_A \sim \frac{x_c^{-A}}{A^{3-\gamma}}$$

where $F(x) = \sum_{A \geq 0} F_A x^A$.

We have now all the necessary material to compute the configuration exponents of all the meandric numbers of interest. Applying the result (4.19)-(4.20) to the central charge (4.17), we find the configuration exponent of the multi-river meander polynomial (4.15)

$$(4.21) \qquad m_{2n}(b, w) \sim \frac{R(b, w)^{2n}}{n^{\alpha(b,w)}}.$$

$$\alpha(b, w) = 2 + \frac{1}{12}\sqrt{1 - c(b, w)}\left(\sqrt{25 - c(b, w)} + \sqrt{1 - c(b, w)}\right).$$

In the particular case of meanders (with one river and one road), we must take $b, w \to 0$, namely $e = f = 1/2$, hence $c(0, 0) = -4$, which yields the exact meander configuration exponent

$$(4.22) \qquad \alpha \equiv \alpha(0, 0) = \frac{29 + \sqrt{145}}{12}.$$

Analogously, the semi-meander configuration exponent may be obtained by studying the singular behavior of a particular correlation function of the B&W model,

leading to

$$(4.23) \qquad \bar{\alpha} = 1 + \frac{1}{24}\sqrt{11}(\sqrt{5} + \sqrt{29}).$$

Note that the arguments of this section do not give any prediction for non-universal quantities such as $R(b, w)$ (which is expected to depend on b and w explicitly, not just on $c(b, w)$). Configuration exponents in physics are usually much more robust, and keep to the same values within large "universality classes" of models. An example here of such a class is that of meanders with tangency points: if we allow the vertex of Fig.17 (b) in the B&W model, say by adding a term of the form $-y \sum_{i,j} B_i^2 W_j^2$ to the potential $V(\{B_i\}, \{W_j\})$ (namely allowing for the vertex of Fig.17 (b), and giving it a weight y), we can now generate meanders whose road may have tangent contact points with the river, and count them as well. Denoting by $\mu_{2n,p}$ the number of tangent meanders with one river and one road, $2n$ crossings and p tangency points, we have the asymptotics for large number k of vertices

$$(4.24) \qquad \sum_{0 \leq n \leq k/2} (y/x)^{k-2n} \mu_{2n,k-2n} \sim \frac{\rho(y/x)^k}{k^\alpha}$$

where α is the same for all finite positive values of y/x, equal in particular to its value at $y = 0$, the meander configuration exponent (4.22). In physical terms, this is a manifestation of the irrelevance of the vertex of Fig.17 (b).

The reasonings of this section, leading in particular to the predictions (4.22) and (4.23), are by no means mathematical proofs, but rely strongly on physical ideas such as those of the Renormalization Group in field theory, which allow us to relate critical singularities and exponents to the details of the models, in particular to their "degrees of freedom" (the height variable here). It would be desirable to have alternative (and more rigorous!) proofs of these results. Let us however mention that these predictions are in perfect agreement (up to 4/5 digits!) with the numerical estimates obtained from the best raw numbers [35] [39].

4.3. Meanders and the Temperley-Lieb Algebra. The most remarkable representation of multi-component meanders is realized by using the domino representation of the Temperley-Lieb algebra $TL_n(\beta)$ defined in (2.17)(2.19), for $\beta = q$. Recall that the elements of $TL_n(\beta)$ are the linear combinations of elementary dominos, obtained by linking their upper and lower lines of n points by pairs, using non-intersecting curves drawn inside the domino. Such a domino is said to be reduced if a maximal use of the relations (2.19) has been made to pull the strings and erase all inner loops. The reduced dominos form a basis of $TL_n(\beta)$ as a vector space. They are in turn expressible as products of generators (2.17) of the form $e_{i_1} e_{i_2} ... e_{i_k}$ with a minimum number k of terms.

We contend that the reduced dominos of $TL_n(\beta)$ are in bijection with the arch configurations of order $2n$, A_{2n}. Given a reduced domino, let us open it up as indicated in Fig.18, so as to bring the lower points $1, 2, .., n$ and upper ones $1', 2', ..., n'$ on a line, in the succession $1, 2, ..., n, n', (n-1)', ..., 2', 1'$. Let us deform the strings connecting these points by pairs, with the constraint of never creating intersections. This produces an arch configuration of order $2n$, whose arches are the deformed strings of the domino. Conversely, we can close any arch configuration of order $2n$ into a reduced domino by bringing half of the bridges, say those numbered $n, n+1, ..., 2n$ on the top line of the domino, in the reverse order.
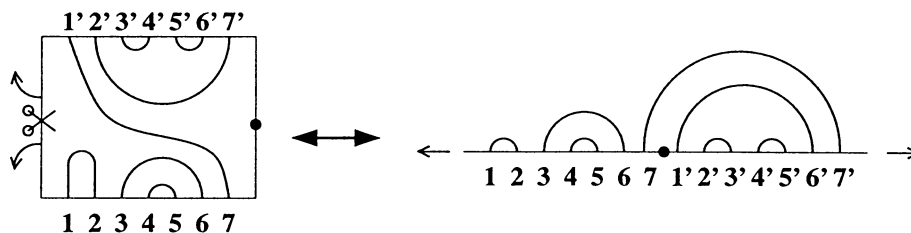
FIGURE 18. The bijection between reduced dominos of $TL_n(\beta)$ and A_{2n} is illustrated in the case $n = 7$. The domino is cut open in order to bring its upper and lower points on a line. The strings are deformed so that no intersection is created. The process is invertible.

Let us now try to interpret the standard trace (2.22) of $TL_n(\beta)$ in terms of arch configurations. Given a domino d, the trace $\mathrm{Tr}(d)$ is simply β^m, where m is the number of distinct loops formed by putting the domino on a cylinder, in which the upper and lower points (i, i') are identified. Assume we have two reduced dominos d_1 and d_2 corresponding respectively to the two arch configurations $a_1, a_2 \in A_{2n}$. Let us compute $\mathrm{Tr}(d_1 d_2^t)$, where d^t stands for the "transpose" of d, namely the domino obtained by reflecting d wrt its lower line of points. Using the mapping to arch configurations, and keeping track of the points (which become bridges), we simply get that

$$(4.25) \qquad \mathrm{Tr}(d_1 d_2^t) \;=\; \beta^{\#\ \mathrm{connected\ \ components\ in\ } \frac{a_1}{a_2^t}} \;=\; \beta^{c(a_1, a_2)}$$

as the identifications of points exactly matching that of bridges when forming the meander equal to the superposition of a_1 and the reflection of a_2. This yields a purely algebraic representation of meanders as pairs of reduced dominos, whose scalar product $(d_1, d_2) = \mathrm{Tr}(d_1 d_2^t) = \beta^{c(a_1, a_2)}$ measures directly the number of connected components. In particular, we have

$$(4.26) \qquad\qquad m_{2n}(\beta) \;=\; \sum_{\substack{d_1, d_2 \ \mathrm{reduced} \\ \mathrm{in}\ TL_n(\beta)}} (d_1, d_2).$$

It actually proves more convenient to use yet another representation for meanders in relation with an ideal of $TL_{2n}(\beta)$ (note the doubling of n). Let $\mathcal{I}_{2n}(\beta)$ denote the left ideal of $TL_{2n}(\beta)$ generated by the element $e_1 e_3 e_5 ... e_{2n-1}$. The reduced elements of this ideal have particularly simple dominos (see Fig.19 for an example): all the lower points $1, 2, ..., 2n$ are connected by consecutive pairs $2i-1 \leftrightarrow 2i$, corresponding to the generators $e_1, e_3, ..., e_{2n-1}$ (2.17) (note that the left ideal property is clear pictorially as concatenating such a domino with any other domino of $TL_{2n}(\beta)$ (from above), which yields a domino with the same property that lower points are linked by consecutive pairs). As loops have been erased, this leaves out only dominos in which the upper points $1', 2', ..., 2n'$ are connected among themselves by pairs. This is nothing but the reflection a^t of some $a \in A_{2n}$, as shown in Fig.19. So the reduced elements of $\mathcal{I}_{2n}(\beta)$ are in straightforward bijection with A_{2n}. Let us make the contact with meanders. Taking two reduced dominos d_1, d_2 respectively
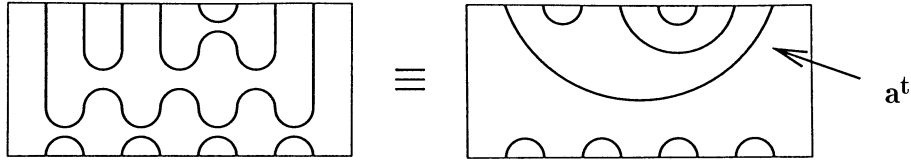
FIGURE 19. The domino corresponding to the element $e_5e_2e_4e_6e_1e_2e_5e_7$ of the ideal $\mathcal{I}_8(\beta)$.

corresponding to $a_1, a_2 \in A_{2n}$, we see that

$$(4.27) \qquad \text{Tr}(d_1 d_2^t) = \beta^{n+c(a_1,a_2)}$$

where the contribution $c(a_1, a_2)$ comes from the superposition of a_1 and a_2^t on the cylinder, while all the arches connecting consecutive pairs simply form n loops, each passing through two bridges. This leads to the representation

$$(4.28) \qquad m_{2n}(\beta) = \sum_{\substack{d_1,d_2 \text{ reduced} \\ \text{in } \mathcal{I}_{2n}(\beta)}} \langle d_1, d_2 \rangle$$

where we have defined $\langle d_1, d_2 \rangle = \beta^{-n}(d_1, d_2) = \beta^{c(a_1,a_2)}$ by use of the scalar product in $TL_{2n}(\beta)$. Note that given any two dominos d_1, d_2 in $\mathcal{I}_{2n}(\beta)$, we have $d_1^t d_2 = \langle d_1, d_2 \rangle d_0$ where $d_0 = e_1 e_3 e_5 ... e_{2n-1}$ is the "fundamental" domino of $\mathcal{I}_{2n}(\beta)$.

4.4. Meander Determinants. The representation (4.28) suggests the introduction of the normalized $c_n \times c_n$ Gram matrix G of the basis of reduced dominos of $\mathcal{I}_{2n}(\beta)$, namely with elements $G_{d_1,d_2} = \langle d_1, d_2 \rangle$, or by using the bijection between the d's and the arch configurations of order $2n$:

$$(4.29) \qquad G_{a_1,a_2} = \beta^{c(a_1,a_2)} \quad a_1, a_2 \in A_{2n}.$$

This matrix contains all the relevant data to study meanders and semi-meanders. In the following, we will sketch the proof of the following remarkable result for the determinant of G:

Theorem 5. *The Gram determinant of the reduced domino basis of $\mathcal{I}_{2n}(\beta)$ reads*

$$(4.30) \qquad \Delta_{2n}(\beta) = \det(G) = \prod_{m=1}^{n} U_m(\beta)^{a_{m,2n}}$$

$$a_{m,2n} = \binom{2n}{n-m} - 2\binom{2n}{n-m-1} + \binom{2n}{n-m-2}$$

where $U_m(2\cos\theta) = \sin(m+1)\theta / \sin\theta$ are the Chebyshev polynomials of the second kind.

The determinant (4.30) is called the meander determinant. The result (4.30) follows from the explicit Gram-Schmidt orthogonalization of G. Before going into this, let us give yet another representation of arch configurations (or reduced dominos of $\mathcal{I}_{2n}(\beta)$), as *walk diagrams*.

A walk diagram of $2n$ steps is a map $h : \{0, 1, ..., 2n\} \to \mathbb{Z}_+$, such that $h(0) = h(2n) = 0$ and $|h(i+1) - h(i)| = 1$ for all i. It can be interpreted as a walk of $2n$ steps of ± 1 on the half-line $\mathbb{Z}_+$, from and to the origin. We may represent such a walk by its piecewise-linear graph, linking the points $(i, h(i))$ in the plane
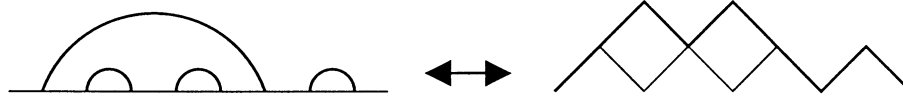
FIGURE 20. The bijection between A_{2n} and W_{2n} is illustrated in the case $n = 4$. We have represented the box decomposition of the corresponding walk diagram $= h_0 + \diamond_2 + \diamond_4$. The corresponding reduced basis element of $\mathcal{I}_8(\beta)$ reads $e_2 e_4 e_1 e_3 e_5 e_7$. The corresponding orthonormal basis element reads $\mu_1 \mu_2 (e_2 - \mu_1)(e_4 - \mu_1) e_1 e_3 e_5 e_7$.

(see Fig.20 for an illustration). Let W_{2n} denote the set of such walk diagrams of $2n$ steps. The sets W_{2n} and A_{2n} are in bijection. Indeed, if $a \in A_{2n}$ let us construct the map $h_a : \{0, 1, ..., 2n\} \to \mathbb{Z}_+$ by first labelling by $0, 1, 2, ..., 2n$ the portions of river respectively to the left of the bridge 1, between the bridges 1 and 2, ..., to the right of the bridge $2n$ of a. Then $h_a(i)$ is defined to be the number of arches passing above the portion i of river. The condition $h_a(0) = h_a(2n) = 0$ is clearly satisfied as there are no arches above the portions 0 and $2n$, and $h_a(i + 1) - h_a(i) = \pm 1$ according to whether an arch originates or terminates at the bridge $i + 1$ (going from left to right). Conversely, we may use these rules to construct an arch configuration from any walk diagram (see Fig.20 for an example). In particular, $|A_{2n}| = |W_{2n}| = c_n$.

The walk diagrams may be constructed by "box additions" on the fundamental diagram h_0 with $h_0(2i) = 0$ for all i. By box addition we mean the following transformation. Let $h \in W_{2n}$ with a minimum at position i, namely such that $h(i - 1) = h(i + 1) = h(i) + 1$. Adding a box to h at position i amounts to letting $h \to h'$, where $h'(j) = h(j)$ for all $j \neq i$, and $h'(i) = h(i) + 2$. We use the notation $h' = h + \diamond_i$. Any walk diagram h has a unique *box decomposition* expressing the box additions to be performed as going from h_0 to h: in Fig.20, we have represented in thin solid lines the two boxes forming the box decomposition of the walk diagram. The order in which these box additions are performed does not matter for distant enough positions i, j when $|i - j| > 1$, but it does for neighboring positions. The reduced dominos of $\mathcal{I}_{2n}(\beta)$ are constructed inductively as follows. Let $d(h)$ be the domino corresponding to the walk $h \in W_{2n}$ (recall the bijection between the reduced dominos and A_{2n}). We have

$$d(h_0) \ = \ d_0 \ = \ e_1 e_3 ... e_{2n-1}$$
$$(4.31) \qquad\qquad d(h + \diamond_i) \ = \ e_i \, d(h).$$

The reduced element corresponding to the arch configuration of Fig.20 reads $e_2 e_4 e_1 e_3 e_5 e_7$, as the box additions are performed at positions 2 and 4.

We are now ready to introduce the Gram-Schmidt change of basis from the reduced dominos, namely a new basis $\delta(h)$, $h \in W_{2n}$, with

$$(4.32) \qquad\qquad \delta(h) \ = \ \sum_{h' \subset h} C_{h,h'} d(h')$$

where the walks $h \in W_{2n}$ have been partially ordered by inclusion, i.e. $h' \subset h$ iff h can be obtained from h' by some box addition(s). This triangular change of basis must also satisfy $\langle \delta(h), \delta(h') \rangle = \delta_{h,h'}$. It turns out that $\delta(h)$ can be constructed inductively in a manner very similar to (4.31). Let us first introduce the notion of *height* of a box addition: we say that a box addition $h' = h + \diamond_i$ is at height m iff
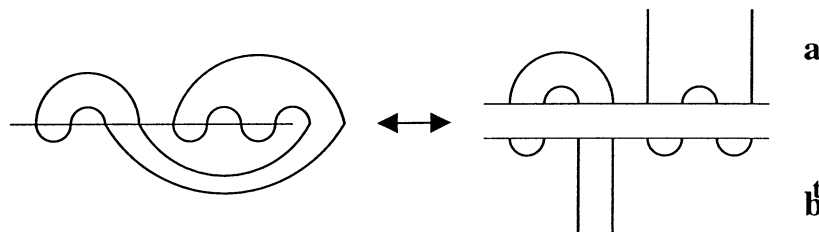
FIGURE 21. A sample semi-meander of order $n = 8$ with winding $w = 2$ is expressed as the superposition of two open arch configurations of order 8 with 2 open arches.

$m = h(i + 1)$, and we denote it by $h' = h + \diamond_{i,m}$. Let us also define the rational fractions

$$(4.33) \qquad \mu_m \equiv \mu_m(\beta) \;=\; \frac{U_{m-1}(\beta)}{U_m(\beta)}$$

in terms of the Chebyshev polynomials of the second kind. The new basis is then constructed inductively as

$$\delta(h_0) \;=\; \mu_1^{n/2} d_0$$

$$(4.34) \qquad \delta(h + \diamond_{i,m}) \;=\; \sqrt{\frac{\mu_{m+1}}{\mu_m}} \big(e_i - \mu_m\big)\, \delta(h).$$

For instance, in the case of the arch configuration of Fig.20, we get the orthonormal basis element $\mu_1 \mu_2 (e_2 - \mu_1)(e_4 - \mu_1)e_1 e_3 e_5 e_7$. The property (4.32) is clearly satisfied by construction, and the orthonormality is proved by induction on the numbers of boxes (see [41] for a detailed proof). The determinant (4.30) follows from a careful collection of all the diagonal $C_{h,h}$ factors, themselves expressible in terms of Chebyshev polynomials, to produce $\det(G) = \prod_{h \in W_{2n}} C_{h,h}^{-2}$.

The meander determinant (4.30) does not however give any direct information as to the meander polynomials (4.5), rather expressed as sums of entries of G. The Gram-Schmidt orthonormalization leads nevertheless to some alternative expressions for these polynomials.

As a final remark, note that the meander determinant can easily be generalized to semi-meanders as follows. Going back to our initial definition of semi-meanders with a semi-infinite river, we may view a semi-meander of order n and winding number w as the superposition of two *open* arch configurations of order n with w open arches, namely arch configurations in which w of the bridges are un-paired, but rather connected to infinity through w vertical half-lines, originating from the un-paired bridges (see Fig.21 for an illustration). When superposing two such objects, we must identify the bridges, and connect the top and bottom open arches starting from the leftmost ones, as indicated in Fig.21. By superposing arbitrary top and bottom open arch configurations of order n with w open arches, we describe the set of multi-component semi-meanders of order n and winding w. Let us denote by $A_n(w)$ the set of open arch configurations of order n with w open arches (note that $n = w \bmod 2$). It is a simple exercise to prove that

$$(4.35) \qquad |A_n(w)| \;=\; c_n(w) \;=\; \binom{n}{\frac{n-w}{2}} - \binom{n}{\frac{n-w}{2} - 1}.$$

As before, for any $a, b \in A_n(w)$, we may introduce the pairing $(a,b) = \beta^{c(a,b)}$, where $c(a,b)$ denotes the number of connected components of road in the semi-meander obtained by superposing a and b^t. Let $G(w)$ be the matrix with entries

$$(4.36) \qquad\qquad G(w)_{a,b} = \beta^{c(a,b)} \quad a, b \in A_n(w).$$

This is the natural counterpart of the meander matrix G for semi-meanders of winding w.

The following result for the determinant of $G(w)$ has been obtained in [31], [41].

Theorem 6.

$$(4.37) \qquad\qquad \det(G(w)) = \prod_{m=1}^{n} U_m(\beta)^{a_{m,n}(w)}$$

$$a_{m,n}(w) = a_{m+\frac{w}{2},n} + w a_{m+\frac{w}{2}-1,n}$$

where the integers $a_{m,n}$ extend those of (4.30) to any integer n and half-integer m such that $n + 2m$ is even, namely

$$(4.38) \qquad\qquad a_{m,n} = c_n(2m) - c_n(2m+2)$$

with $c_n(w)$ as in (4.35).

4.5. Generalizations. The meanders can be generalized along two other very different lines, both using generalizations of the Temperley-Lieb algebra. The first one is inspired by the theory of integrable lattice models based on $sl(N)$, whereas the Temperley-Lieb algebra really is linked to $sl(2)$ in this language. The second one consists in "coloring" the Temperley-Lieb algebra, namely defining an algebra generated by dominos with colored strings respecting certain patterns, the Fuss-Catalan algebras. Both generalizations give rise to generalized meander determinant formulas.

sl(N) meanders: The Temperley-Lieb algebra is the first non-trivial member of a sequence of factors of the Hecke algebra by the so-called q-antisymmetrizers of order N, $N = 2$ (TLA), 3, ... More precisely, the Hecke algebra $H_n(q)$ is generated by elements $1, T_1, T_2, ..., T_{n-1}$, subject to the relations

$$(4.39) \qquad \begin{aligned} (T_i + 1)(T_i - q^2) &= 0 \\ T_i T_j &= T_j T_i \quad \text{for } |i - j| > 1 \\ T_i T_{i+1} T_i &= T_{i+1} T_i T_{i+1}. \end{aligned}$$

This is a q-deformation (q is a complex parameter) of the braid algebra of the symmetric group (where $T_i \to (i, i+1)$ and $q \to 1$), and as such it is possible to define for any $\sigma \in S_n$, the element

$$(4.40) \qquad\qquad T_\sigma = T_{i_1} T_{i_2} ... T_{i_k}$$

where the permutation $\sigma = (i_1, i_1 + 1)(i_2, i_2 + 1)...(i_k, i_k + 1)$ with a minimal number $k = \ell(\sigma)(=$length of $\sigma)$ of factors. Let m_N be the maximal such length of the elements of S_N. The q-antisymmetrizers of order N then read

$$(4.41) \qquad\qquad A_N(T_1, T_2, ..., T_N) = q^{M_N} \sum_{\sigma \in S_{N+1}} (-q^2)^{-\ell(\sigma)} T_\sigma$$

together with the corresponding translations of all the T indices by i, $i = 0, 1, ..., n - N - 1$. In particular we have

$$(4.42) \qquad A_1(T_1) = q - q^{-1}T_1$$
$$A_2(T_1, T_2) = q^3 - q(T_1 + T_2) + q^{-1}(T_1T_2 + T_2T_1) - q^{-3}T_1T_2T_1$$

for $N = 1, 2$. The N-th quotient of the Hecke algebra $H_n^{(N)}(q)$ is that of the Hecke algebra $H_n(q)$ by the ideal generated by the q-antisymmetrizers of order N, namely $A_N(T_i, T_{i+1}, ..., T_{i+N-1})$, $i = 1, 2, ..., n - N$. The algebras $H_n^{(N)}(q)$ play a central role in the definition of integrable lattice models based on $sl(N)$. It was actually shown that $H_n^{(N)}(q)$ commutes with the quantum enveloping algebra $U_q(sl(N))$, acting on a tensor product of n fundamental representations.

It turns out that $H_n^{(2)}(q) = TL_n(\beta)$, with $\beta = q + q^{-1}$. Indeed, defining $e_i = A_1(T_i) = q - q^{-1}T_i$, the q-antisymmetrizer of order 2 simply becomes $Y_2(e_i, e_{i+1}) = A_2(T_i, T_{i+1}) = e_i e_{i+1} e_i - e_i$, while the quadratic relation in (4.39) reads $e_i(e_i - \beta) = 0$. Analogously, we denote by $Y_N(e_i, ..., e_{i+N-1}) = A_N(T_i, ..., T_{i+N-1})$. We are going to generalize the picture of a meander thought of as a pair of reduced elements of the ideal $\mathcal{I}_{2n}(\beta) = e_1 e_3 ... e_{2n-1} TL_{2n}(\beta)$. We introduce the left ideal of $H_{Nn}^{(N)}(q)$

$$(4.43) \qquad \mathcal{I}_{Nn}^{(N)}(\beta) = \prod_{i=0}^{n-1} Y_{N-1}(e_{Ni+1}, e_{Ni+2}, ..., e_{Ni+N-1}) H_{Nn}^{(N)}(q).$$

A generalized $sl(N)$ meander is a pair of reduced elements of the ideal (4.43). By reduced, we mean an element obtained as a minimal product of generators e_i, multiplied by the fundamental element $Y_0 = \prod_{i=0}^{n-1} Y_{N-1}(e_{Ni+1}, e_{Ni+2}, ..., e_{Ni+N-1})$. A simple enumeration of these reduced elements using generalized walk diagrams gives the dimension of (4.43) as a vector space: $d_{Nn}^{(N)} = (Nn)! \prod_{i=0}^{N-1} i!/(n+i)!$ (see [42] for details). This is known as a N-dimensional Catalan number.

The Hecke algebra quotient $H_n^{(N)}(q)$ is equipped with a standard Markov trace such that $\text{Tr}(1) = U_{N-1}(\beta)$ (U the Chebyshev polynomials of the second kind), and

$$(4.44) \qquad \text{Tr}(E(e_1, ..., e_{i-1})e_i) = \mu_{N-1}(\beta) \, \text{Tr}(E(e_1, ..., e_{i-1}))$$

for any element E involving only the generators $e_1, e_2, ..., e_{i-1}$. Noting that $Y_0^t Y_0 = \gamma_N^{-n} Y_0$, with $\gamma_{N+1}/\gamma_N^2 = \mu_N$, $\gamma_1 = \mu_1$, we may define the Gram matrix G with entries

$$(4.45) \qquad G_{a,b} = \gamma_N^n \, \text{Tr}(a^t b) \quad a, b \text{ reduced.}$$

The determinant of this matrix is the generalized sl(n) meander determinant. It has been computed in [42], and found to take the form

$$(4.46) \qquad \Delta_{Nn} = \prod_{m=1}^{n+N-2} U_m(\beta)^{d_{m,Nn}}$$

where the $d_{m,Nn}$ are some integers, related to some path counting on the Weyl chamber of $sl(N)$ (the generalization of the integer half-line $\mathbb{Z}_+$). The strategy of the proof is essentially the same as for the $N = 2$ case, and relies on the explicit Gram-Schmidt orthonormalization of the basis of reduced elements [42].

Colored meanders: Coloring the Temperley-Lieb algebra [43] amounts to the following generalization of the dominos: they must have Nn upper and lower points,

now colored with N distinct colors numbered say $1, 2, ..., N$. The pattern of coloring of successive upper and lower points is $1, 2, 3, ..., N, N, N-1, ..., 2, 1, 1, 2, 3, ...$ and ends up with N if n is odd and 1 otherwise. The dominos are further subject to the N-coloring condition that only points of the same color can be connected by a string, which is then painted with the same color as its ends. As before, all the points must be connected through non-intersecting strings within the rectangle of the domino. To form an algebra, we must define the multiplication of dominos. This is done as before by concatenation, by identifying the lower points of the first domino with the upper ones of the second. Then any contractible loop of a given color i may be erased and replaced by a factor of α_i, where $\alpha_1, \alpha_2, ..., \alpha_N$ are N given complex parameters. With these definitions, the reduced N-colored dominos (those without inner loops) form a basis of the N-color Fuss-Catalan algebra $FC_n(\alpha_1, \alpha_2, ..., \alpha_N)$. Enumerating those dominos, one gets the dimension of this algebra as a vector space: $f_{Nn}^{(N)} = \binom{(N+1)n}{n}/(Nn+1)$. These are the generalized Catalan numbers. We clearly have $TL_n(\beta) = FC_n(\alpha = \beta)$ for $N = 1$.

This suggests defining the N-colored meanders of order $2Nn$ to be meanders of order $2Nn$, whose $2Nn$ bridges are painted according to the above pattern, and such that only bridges of the same color are connected by arches. In turn, this describes interlocked polymers of different colors. As before, we will relate the colored meanders to pairs of reduced elements of some ideal of $FC_{2n}(\alpha_1, ..., \alpha_N)$. First we need to write a system of generators for $FC_n(\alpha_1, ..., \alpha_n)$. The simplest presentation is through the embedding into $TL_n(\alpha_1) \otimes TL_n(\alpha_2) \otimes ... \otimes TL_n(\alpha_N)$, with, in addition to the identity $1 = 1 \otimes ... \otimes 1$, the following generators

$$(4.47) \quad U_i^{(m)} = \begin{cases} 1 \otimes 1 \otimes ... \otimes 1 \otimes e_i^{(k-m+1)} \otimes e_i^{(k-m+2)} \otimes ... \otimes e_i^{(k)} & \text{if } i \text{ odd} \\ e_i^{(1)} \otimes e_i^{(2)} \otimes ... \otimes e_i^{(m)} \otimes 1 \otimes 1 \otimes ...... \otimes 1 & \text{if } i \text{ even} \end{cases}$$

for $i = 1, 2, ..., n-1$, $m = 1, 2, ..., N$, and where $e_i^{(j)}$ denotes the generator e_i of the j-th factor $TL_n(\alpha_j)$, corresponding to the strings of color i. The relations between these generators are direct consequences of (2.19) in each factor (see [44] for the detailed relations). Let us now consider the left ideal

$$(4.48) \qquad \mathcal{I}_{2n}(\alpha_1, ..., \alpha_N) = U_1^{(N)} U_3^{(N)} ... U_{2n-1}^{(N)} FC_{2n}(\alpha_1, ..., \alpha_N).$$

The dominos generating it are very simple: all their lower points are connected among themselves, the point $2Ni + j$ of color j being connected with $2N(i+1) + 1 - j$, $i = 0, 1, ..., n-1$, $j = 1, 2, ..., N$. Hence their upper points are all connected among themselves, through N-colored arch configurations of order $2Nn$, in number $f_{Nn}^{(N)}$. The basis of reduced dominos is therefore in bijection with these arch configurations. The trace of the Temperley-Lieb algebra extends trivially to the Fuss-Catalan algebras. Noting that $(U_i^{(N)})^2 = \alpha_1 \alpha_2 ... \alpha_N U_i^{(N)}$, we may further define a Gram matrix $G^{(N)}$ of size $f_{Nn}^{(N)} \times f_{Nn}^{(N)}$ with entries

$$(4.49) \qquad G_{a,b}^{(N)} = (\alpha_1 \alpha_2 ... \alpha_N)^{-n} \text{Tr}(a^t b) \quad a, b \text{ reduced}$$

called the N-color meander determinant.

Working out the explicit Gram-Schmidt orthonormalization of the reduced basis of the ideal (4.48), one finds the following result for the N-color meander determinant

$$D_{2Nn}^{(N)}(\alpha_1, ..., \alpha_N) \; = \; \det(G^{(N)}) \; = \; \prod_{j=1}^{N} \Delta_N(\alpha_j)$$

(4.50) $$\Delta_N(\alpha) \; = \; \prod_{m=1}^{n} \big(U_m(\alpha)\big)^{a_{m,n}^{(N)}}$$

$$a_{m,n}^{(N)} \; = \; \binom{(N+1)n}{n-m} - 2\binom{(N+1)n}{n-m-1} + \binom{(N+1)n}{n-m-2}.$$

We recover (4.30) as the particular case $N = 1$.

An interesting point is that, while the algebraic structure underlying the $sl(N)$ meanders borrows from known integrable models, that of the N-colored ones actually gives rise to new two-dimensional integrable lattice models of fully-packed colored loops [44]. More precisely, the Fuss-Catalan algebra allows for the construction of new solutions to the Yang-Baxter equation, leading to new integrable lattice models.

5. Conclusion

In this expository paper, we have reviewed various techniques used to study the folding problem of (phantom) tethered and fluid membranes respectively modelled by foldable lattices and foldable tessellations. In both studies, we have considered the folding of *two-dimensional* objects with the possibility of interpenetrating themselves. In both cases, and in a rather unrelated way, we have unearthed some kind of integrable structure, whether it be simply the integrability of the associated lattice model or a Temperley-Lieb algebra structure in the first case, or the existence of integrable discrete equations (or integrable partial differential equations, in the thermodynamic limit) for the second. Both turn out to be intimately linked, as the Discrete Hirota equations we found can be used to reformulate the Bethe Ansatz equations of the integrable lattice models [20].

In the third study, we have simplified the object we were folding into a one-dimensional polymer chain, but we have complicated the folding itself by requiring that the polymer be self-avoiding and not phantom. The main achievement there (though the less rigorous one) is probably the predictions for the exact values of meandric configuration exponents. These results certainly await mathematical proofs, but the amount of work they require is probably formidable. Another important result of our study is the explicit realization of an underlying Temperley-Lieb algebra structure in meanders which provides us with a sort of common denominator with the preceding two cases.

In addition to the various generalizations of meanders presented here, the most exciting would really be the self-avoiding folding problem of two-dimensional objects (even the square lattice is quite elusive, as one can convince oneself easily by experimenting with a sheet of paper). We expect it to possess some sort of underlying generalized Temperley-Lieb algebra structure, which might have to do with attempts at generalizing the notion of integrability to higher dimensional lattice models (e.g. such as the so-called tetrahedron equation [45] in three dimensions).

References

[1] Y. Kantor and D.R. Nelson, *Crumpling Transition in Polymerized Membranes*, Phys. Rev. Lett. **58** (1987) 2774 and *Phase Transitions in Flexible Polymeric Surfaces*, Phys. Rev. **A 36** (1987) 4020.

[2] D.R. Nelson and L. Peliti, *Fluctuations in Membranes with Crystalline and Hexatic Order*, J. Physique **48** (1987) 1085.

[3] M. Paczuski, M. Kardar and D.R. Nelson, *Landau Theory of The Crumpling Transition*, Phys. Rev. Lett. **60** (1988) 2638.

[4] F. David and E. Guitter, *Crumpling Transition in Elastic Membranes: Renormalization Group Treatment*, Europhys. Lett. **5** (1988) 709.

[5] M. Baig, D. Espriu and J. Wheater, *Phase Transitions in Random Surfaces*, Nucl. Phys. **B314** (1989) 587; R. Renken and J. Kogut, *Scaling Behavior at the Crumpling Transition*, Nucl. Phys. **B342** (1990) 753; R. Harnish and J. Wheater, *The Crumpling Transition of Crystalline Random Surfaces*, Nucl. Phys. **B350** (1991) 861; J. Wheater and P. Stephenson, *On the Crumpling Transition in Crystalline Random Surfaces*, Phys. Lett. **B302** (1993) 447.

[6] Y. Kantor and M.V. Jarić, *Triangular Lattice Foldings—a Transfer Matrix Study*, Europhys. Lett. **11** (1990) 157-161.

[7] P. Di Francesco and E. Guitter, *Entropy of Folding of the Triangular Lattice*, Europhys. Lett. **26** (1994) 455.

[8] M. Bowick, P. Di Francesco, O. Golinelli and E. Guitter, *3D folding of the triangular lattice*, Nucl. Phys. **B450[FS]** (1995) 463-494. MR **97a:**82014

[9] P. Di Francesco and E. Guitter, *Folding Transition of the Triangular Lattice*, Phys. Rev. **E50** (1994) 4418-4426.

[10] P. Di Francesco, E. Guitter and S. Mori, *Folding of the triangular lattice with quenched bending rigidity*, Phys. Rev. **E 55** No. 1 (1997) 237-251.

[11] P. Di Francesco, *Folding Transitions of the Square-Diagonal Lattice*, Nucl. Phys. **B528** (1998) 453-468. MR **99h:**82029

[12] R.J. Baxter, *Colorings of a Hexagonal Lattice*, J. Math. Phys. **11** (1970) 784-789, MR **42:**1457; and *q-Colourings of the Triangular Lattice*, J. Phys. **A19** Math. Gen. (1986) 2821-2839. MR **87k:**82123

[13] P. Di Francesco, *Folding the Square-Diagonal Lattice*, Nucl. Phys. **B525[FS]** (1998) 507-548. MR **99k:**82033

[14] H. Temperley and E. Lieb, *Relations between the Percolation and Coloring Problems and other Graph-Theoretical Problems Associated with Regular Planar Lattices: Some Exact Results for the Percolation Problem*, Proc. Roy. Soc. **A322** (1971) 251-280 MR **58:**16425; see also the book by P. Martin, *Potts Models and Related Problems in Statistical Mechanics*, World Scientific, Singapore (1991) for a review. MR **92m:**82030

[15] R.J. Baxter, *Exactly Solved Models in Statistical Mechanics*, Academic Press, London (1982). MR **86i:**82002a

[16] This problem is discussed in the mathematical entertainment section, edited by A. Shen, of the Mathematical Intelligencer, Volume 19 number 4 (1997) 48.

[17] P. Di Francesco, P. Ginsparg and J. Zinn–Justin, *2D Gravity and Random Matrices*, Physics Reports **254** (1995) 1-131. MR **96c:**81191

[18] P. Di Francesco, B. Eynard and E. Guitter, *Coloring Random Triangulations*, Nucl. Phys. **B516[FS]** (1998) 543-587. MR **2000c:**82039

[19] B. Eynard and C. Kristjansen, *An iterative solution of the 3-color problem on a random lattice*, Nucl. Phys. **B516[FS]** (1998) 592-542. CMP 98:13

[20] I. Krichever, O. Lipan, P. Wiegmann and A. Zabrodin, *Quantum integrable systems and elliptic solutions of classical discrete nonlinear equations*, Comm. Math. Phys. **188** (1997) 267. MR **99c:**58076

[21] C. Itzykson and J.-B. Zuber, *The planar approximation II*, J. Math. Phys. **21** (1980) 411. MR **81a:**81068

[22] Harish-Chandra, *Differential operators on a semi-simple Lie algebra*, Amer. Jour. of Math **79** (1957) 87 MR **18:**809d; J. Duistermaat and G. Heckman, *On the variation of cohomology of the symplectic form of the reduced phase space*, Inv. Math. **69** (1982) 259-268. MR **84h:**58051a

[23] W. Tutte, *A Census of Planar Maps*, Canad. Jour. of Math. **15** (1963) 249. MR **26:**4343

[24] A. Sainte-Laguë, *Avec des nombres et des lignes (Récréations Mathématiques)*, Vuibert, Paris (1937).

[25] J. Touchard, *Contribution à l'étude du problème des timbres poste*, Canad. J. Math. **2** (1950) 385-398. MR **12:**312i

[26] W. Lunnon, *A map-folding problem*, Math. of Comp. **22** (1968) 193-199. MR **36:**5009

[27] V. Arnold, *The branched covering of $CP_2 \to S_4$, hyperbolicity and projective topology*, Siberian Math. Jour. **29** (1988) 717-726. MR **90a:**57037

[28] K.H. Ko, L. Smolinsky, *A combinatorial matrix in 3-manifold theory*, Pacific. J. Math **149** (1991) 319-336. MR **92d:**57008

[29] S. Lando and A. Zvonkin, *Plane and projective meanders*, Theor. Comp. Sci. **117** (1993) 227-241 MR **94i:**05004; and *Meanders*, Selecta Math. Sov. **11** (1992) 117-144. MR **93k:**05013

[30] P. Di Francesco, O. Golinelli and E. Guitter, *Meander, Folding and Arch Statistics*, Math. Comput. Modelling, Vol. **26**, No.8-10 (1997) 97-147. MR **99f:**82029

[31] P. Di Francesco, O. Golinelli and E. Guitter, *Meanders and the Temperley-Lieb Algebra*, Commun. Math. Phys. **186** (1997), 1-59. MR **99f:**82028

[32] R. Bacher, *Meander Algebras*, prépublication de l'Institut Fourier n° 478 (1999).

[33] P. Di Francesco, O. Golinelli and E. Guitter, *Meanders: a direct enumeration approach*, Nucl. Phys. **B482[FS]** (1996), 497-535. MR **97j:**82074

[34] O. Golinelli, *A Monte-Carlo study of meanders*, preprint cond-mat/9906329, to appear in EPJ **B** (2000).

[35] I. Jensen, *Enumeration of plane meanders*, preprint cond-mat/9910313.

[36] P. Di Francesco, O. Golinelli and E. Guitter, *Meanders: exact asymptotics*, preprint cond-mat/9910453, to appear in Nucl. Phys. **B** (2000).

[37] P. Di Francesco, *Matrix model combinatorics: applications to folding and coloring*, M.S.R.I. lecture notes, preprint math-ph/9911002 (1999).

[38] J. Jacobsen and J. Kondev, *Field theory of compact polymers on the square lattice*, Nucl. Phys. **B 532** [FS], (1998) 635-688 MR **99f:**82027; *Transition from the compact to the dense phase of two-dimensional polymers*, J. Stat. Phys. **96**, (1999) 21-48.

[39] P. Di Francesco, E. Guitter and J. Jacobsen, work in progress.

[40] V.G. Knizhnik, A.M. Polyakov and A.B. Zamolodchikov, *Fractal Structure of 2-D Quantum Gravity*, Mod. Phys. Lett. **A3** (1988) 819, MR **89i:**83039; F. David, *Conformal Field Theories Coupled to 2-D Gravity in the Conformal Gauge*, Mod. Phys. Lett. **A3** (1988) 1651, MR **89k:**81138; J. Distler and H. Kawai, *Conformal Field Theory and 2-D Quantum Gravity or Who's Afraid of Joseph Liouville?*, Nucl. Phys. **B321** (1989) 509. MR **90g:**81226

[41] P. Di Francesco, *Meander Determinants*, Commun. Math. Phys. **191** (1998) 543-583. MR **99e:**05007

[42] P. Di Francesco, *SU(N) Meander Determinants*, Jour. Math. Phys. **38** (1997) 5905-5943. MR **99k:**05019

[43] D. Bisch and V. Jones, *Algebras associated to intermediate subfactors*, Inv. Math. **128** (1997) 89-157. MR **99c:**46072

[44] P. Di Francesco, *New Integrable Lattice Models from Fuss-Catalan Algebras*, Nucl. Phys. **B532** (1998) 609-634. MR **99k:**82020

[45] A.B. Zamolodchikov, *Tetrahedron Equations and the Relativistic S-Matrix of Straight Strings in $(2+1)$-Dimensions*, Commun. Math. Phys. **79** (1981) 489-505. MR **82k:**81081

SERVICE DE PHYSIQUE THÉORIQUE, C.E.A. SACLAY, F-91191 GIF SUR YVETTE, FRANCE
E-mail address: `philippe@spht.saclay.cea.fr`